Real Testbed Implementation and Performance Analysis of Power Domain Non-Orthogonal Multiple Access Technique using Wireless Access Research Platform

*A thesis submitted towards partial fulfilment of the
requirements for the degree of*
**Master of Engineering in
Electronics and Telecommunication Engineering**

Submitted by
**RAKHI MONDAL
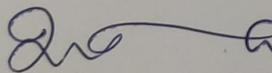Roll No. 00201070206
Registration No. 154075 of 2020-21**

Under the guidance of
**Prof. Iti Saha Misra
Department of Electronics and Telecommunication Engineering
Jadavpur University
Kolkata 700032**

**Faculty of Engineering and Technology
Jadavpur University
Kolkata 700032
June 2022**

M.E. (Electronics and Telecommunication Engineering) course affiliated to

Faculty of Engineering and Technology Jadavpur University

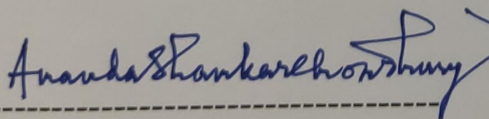Kolkata, India

CERTIFICATE OF RECOMMENDATION

This is to certify that the dissertation entitled **"Real Testbed Implementation and Performance Analysis of Power Domain Non-Orthogonal Multiple Access Technique Using Wireless Access Research Platform"** has been carried out by **RAKHI MONDAL** (University Registration No: 154075 of 2020-2021), Class Roll No. **002010702006** under the guidance and supervision of Prof. Iti Saha Misra and be accepted in partial fulfilment of the requirements for the degree of Master of Engineering in Electronics and Telecommunication Engineering. The research results presented in the thesis have not been included in any other places submitted for any degree to any other University or Institute.

_____ 27.06.2022

DR. ITI SAHA MISRA
PROFESSOR
Dept. of ETCE
JADAVPUR UNIVERSITY
Kolkata - 700 032

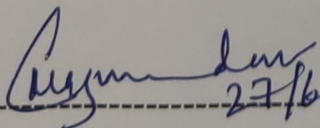(Prof. Iti Saha Misra) SUPERVISOR

Department of Electronics & Telecommunication Engineering Jadavpur University

Kolkata -700032

_____ 27.06.2022

ANANDA SHANKAR CHOWDHURY
Professor and Head
Electronics and Telecommunication Engineering
Jadavpur University, Kolkata-32

(Prof. Ananda Shankar Chowdhury) HOD

Department of Electronics & Telecommunication Engineering

Jadavpur University, Kolkata-700 032

_____ 27/6/2022

(Prof. Chandan Mazumdar) DEAN

Faculty Council of Engineering & Technology

Jadavpur University, Kolkata-700 032

DEAN
Faculty of Engineering & Technology
JADAVPUR UNIVERSITY
KOLKATA-700 032

M.E. (Electronics and Telecommunication Engineering) course affiliated to

Faculty of Engineering and Technology

Jadavpur University Kolkata, India

<u>CERTIFICATE OF APPROVAL</u> **

This foregoing thesis is hereby approved as a credible study of an engineering subject carried out and presented in a manner satisfactorily to warranty its acceptance as a prerequisite to the degree for which it has been submitted. It is understood that by this approval the undersigned do not endorse or approve any statement made or opinion expressed or conclusion drawn therein but approve the thesis only for purpose for which it has been submitted.

External Examiner

Internal Examiner

** Only in case the thesis is approved.

DECLARATION OF ORIGINALITY AND COMPLIANCE OF ACADEMIC ETHICS

I hereby declare that this thesis contains literature survey and original research work by the undersigned candidate, as part of his **Master of Engineering in Electronics and Telecommunication Engineering** studies during academic session 2021- 2022.

All information in this document has been obtained and presented in accordance with academic rules and ethical conduct.

I also declare that, as required by this rules and conduct, I have fully cited and referred all material and results that are not original to this work.

NAME: **RAKHI MONDAL**

EXAM ROLL NUMBER: **M4ETC22006**

CLASS ROLL NUMBER: **002010702006**

THESIS TITLE: **Real Testbed Implementation and Performance Analysis of Power Domain Non-Orthogonal Multiple Access Technique Using Wireless Access Research Platform**

_____   _____

SIGNATURE   DATE

Acknowledgement

I would like to express my deepest gratitude to my supervisor Prof. Iti Saha Misra for her valuable guidance, active supervision and innovative ideas that make it possible to prepare this thesis paper. Her advices will help me in future research work. I am privileged to witness her enthusiastic and dedicated interest towards advanced research that motivates me and enriches my growth as a student and a researcher.

I would like to convey my heartfelt thanks to my junior Ms. Sayanti Jana for her generous assistance and interest in the topic I have worked. Some important discussions with her really enhances the quality of generating data and results for the thesis.

I would like to thank the entire dept. of Electronics and Telecommunication Engineering and all the people, who directly and indirectly helped me to achieve one of the major goals of my life.

Last but not the least; I remain ever grateful to my parents who provided me with never-ending support and encouragement during all my years in academia.

Place: Kolkata
Date: **(Ms. Rakhi Mondal)**
Electronics and
Telecommunication
Engineering
Jadavpur University

Abstract

The Radio Access Technologies (RATs) refer to Multiple Access (MA) techniques which play an important role in distributing radio resources among users. Non-orthogonal multiple access (NOMA) is a promising radio access technology for 5G cellular networks which outperforms the conventional multiple access technique to meet the requirement of maximizing spectral efficiency and minimizing latency through multiplexing users in the power domain. As NOMA can serve multiple users with different channel conditions simultaneously, it aims to improve users' fairness and higher massive connectivity. According to the literature survey, NOMA has been included in third generation partnership project long term evolution advanced (3GPP LTE Release 13). It is also compatible with the current and future communication systems since it does not require significant modifications on the existing architecture. NOMA is classified as power-domain and code-domain. This thesis primarily focuses on power domain NOMA (PD-NOMA) that utilizes superposition coding (SC) at the transmitter and successive interference cancellation (SIC) at the receiver. In this thesis, a detailed performance analysis with respect to BER and Sum Capacity of downlink PD- NOMA with two users as well as three users is presented under various modulation schemes such as BPSK (Binary) QPSK (Quadrature) Phase Shift Keying and combination of BPSK and QPSK i.e., an adaptive modulation approach using fixed and constrained optimization-based power allocation techniques in consideration with different fairness factor values. Along with the simulation a real time testbed implementation of downlink Power Domain NOMA (PD-NOMA) has been conducted using the Software Defined Radio (SDR) kit, Wireless Access Research Platform (WARP) for the performance analysis with respect to Bit Error Rate (BER) under various modulation schemes using fixed power allocation technique .WARP v3 is the latest generation of WARP hardware, integrating a high performance FPGA, flexible RF interfaces and multiple peripherals to facilitate rapid prototyping of custom wireless designs transmitting in both the 2.4 GHz and 5GHz range. A comparative analysis of the BER performance of PD-NOMA with two users considering different modulation schemes are also provided in this paper.

<u>Table of Contents</u>

Chapter 4
Real Time Implementation of PD NOMA using WARP: A Software Defined Radio Kits

Chapter 5
Conclusion and Future Works

Abbreviations

AGC	Automatic Gain Control
AWGN	Additive White Gaussian Noise
BER	Bit Error Rate
BPSK	Binary Phase Shift Keying
CFO	Carrier Frequency Offset
CSI	Channel State Information
IFFT	Inverse Fast Fourier Transform
LTS	Long Training Symbol
OFDM	Orthogonal Frequency Division Multiplexing
PD-NOMA	Power Domain Non-Orthogonal Multiple Access
QPSK	Quadrature Phase Shift Keying
SC	Superposition Coding
SDR	Software Defined Radio
SFO	Sampling Frequency Offset
SIC	Successive Interference Cancellation
SNR	Signal to Noise Ratio
STS	Short Training Symbol
WARP	Wireless Access Research Platform

List of Tables

List of Figures

Chapter 1   **Introduction**

1.1   Introduction

Wireless mobile communication system has become an essential part of modern lives. The significant increase in the number of devices leads to reuse the same radio spectrum several times by different applications or users. Recently, development of suitable techniques that may be integrated in next generation wireless communication systems is undertaken by the researchers in order to fulfil the fundamental and imminent requirements, including very high spectral efficiency, very low latency, very high achievable data rate, massive device connectivity, ultra-high reliability, excellent user fairness, high throughput, supporting diverse quality of services (QoS), energy efficiency, and a considerable reduction in the cost [1]. Some potential technologies have been put forward by the academia and the industry in order to satisfy the aforementioned stringent requirements and to address the challenges of future generations. For example, millimetre wave (mm Wave) technology was suggested to enlarge the transmission bandwidth for very high speed communications [2], massive multiple input multiple output (MIMO) concept was presented to improve capacity and energy efficiency [3], and ultra-dense networks were introduced to increase the throughput and to reduce the energy consumption through using a large number of small cells [4].

Multiple access (MA) techniques play a major role in the overall communication process. As seen in Fig.1.1, starting from the first generation until fourth, Orthogonal Multiple Access (OMA) techniques such as Frequency Division Multiple Access (FDMA), Time Division Multiple Access (TDMA), Code Division Multiple Access (CDMA) and Orthogonal Frequency Division Multiple Access (OFDMA) have been used [5,6]. In order to meet the

requirement of high data rates, low latency and massive user connectivity, a promising MA technology, referred to as NOMA, comes into the picture. In general, NOMA schemes can be classified into two types: power-domain multiplexing and code-domain multiplexing. In power-domain multiplexing, different users are allocated different power coefficients according to their channel conditions in order to achieve a high system performance. PD-NOMA adopts superposing multiple users in the power domain and makes use of channel gain difference between multiplexed users. It employs superposition coding (SC) at the transmitter side and successive interference cancellation (SIC) at the receiver. In [7], the authors have studied users' pairing which concludes that the performance of NOMA is better than that of OMA, especially with users having more typical channel conditions. The power allocation strategy among users in PD-NOMA is studied in [8]. In PD-NOMA, the user nearer to the base station (BS) and having better channel condition is given less power rather than the far users who have poor channel condition. In case of code-domain multiplexing NOMA, different users are allocated to different type of codes and multiplexed over the same time-frequency resources, such as multiuser shared access (MUSA) [9], sparse code multiple access (SCMA) [10], and low-density spreading (LDS) [11]. In addition to power-domain multiplexing and code-domain multiplexing, there are several other NOMA schemes which include pattern division multiple access (PDMA) [12] and bit division multiplexing (BDM) [13]. Although code-domain multiplexing has a potential to augment the spectral efficiency, it requires a high transmission bandwidth which is not easily applicable to the current systems. On the other hand, power-domain multiplexing has an easy implementation which adopts no considerable changes on the existing networks. Also, it does not require additional bandwidth in order to improve spectral efficiency [14]. In this thesis, we will focus on the power-domain NOMA.
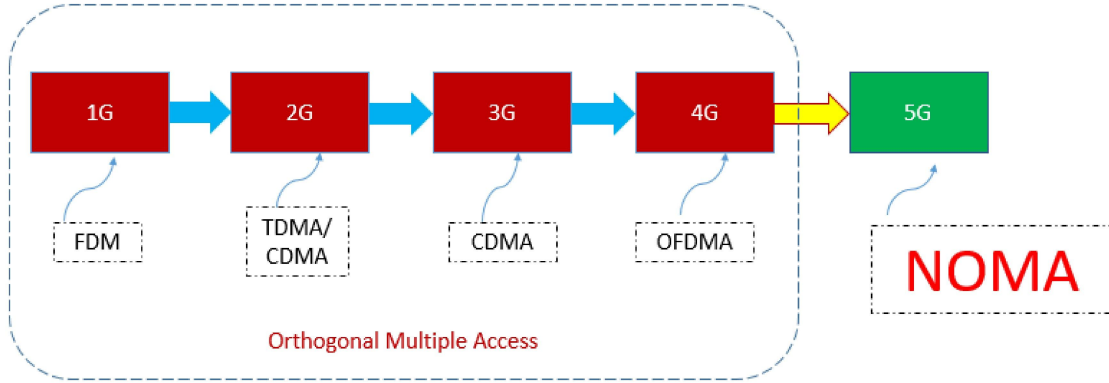
Fig.1.1. Different Multiple Access Technologies for cellular systems

Another insight of this paper is the RF-FPGA board, named Wireless Open Access Research Platform (WARP), which is controllable by generic programming codes over a user-friendly MATLAB interface. It can provide a flexible and adaptive FPGA transceiver platform that can be configured into the required system. MATLAB codes can be used to handle the transmission, reception and processing of the signal to capture useful information to study and improve the system.

1.2 Objective

According to the literature survey, NOMA is a promising solution to meet the requirements of 5G communication such as high data rates, low latency and massive user connectivity. So, the main objective of this thesis is to implement a PD-NOMA-OFDM system using a real testbed i.e., Wireless Access Research Platform (WARP) transceiver kits and analyse the system performance with respect to bit error rate (BER). In order to make a proper trade-off between the bit error rate (BER) and throughput, the type of digital modulation scheme, employed in the system, plays an important role. In case of PD-NOMA if higher order modulation schemes are applied to users who are considerably far from the base station, then there is a high chance of increased BER for those users' data.

Hence, higher order modulation schemes are preferred to be applied on users near to the base station. The system performance analysis is observed under different modulation techniques (BPSK, QPSK and Adaptive approach).

1.3 Literature Survey

NOMA has been incorporated in third generation partnership project long term evolution advanced (3GPP LTE Release 13) [15– 21]. To be more specific, in this standard, a downlink version of NOMA has utilized multiuser superposition transmission (MUST) technique [15]. MUST makes use of the superposition coding concept for a multiuser transmission in LTE-A systems. While using MUST, the deployment scenarios, evaluation methodologies, and candidate NOMA scheme in 3GPP radio access network (RAN) have been investigated in [16–18]. Then system level performance and link level performance of NOMA have been analysed in [19, 20], respectively. Next, 3GPP LTE Release 14 has been proposed [21], in which intra-cell interference is stamped out and hence LTE is able to reinforce downlink intra-cell multiuser superposition transmission. Also, layered division multiplexing (LDM) NOMA, is used in the future digital TV standard, ATSC 3.0 [22]. Furthermore, the standardization survey of NOMA schemes for 5G New Radio (NR) continues within 3GPP LTE Release 15 [23]. The undertaken objectives in Release 15 can be summarized as follows: (1) transmitter side signal processing schemes for NOMA, such as modulation and symbol level processing, coded bit level processing, and symbol to resource element mapping; (2) receivers for NOMA, such as minimum mean-square error (MMSE) receiver, SIC and/or parallel interference cancellation (PIC) receiver, joint detection type receivers, and complexity of the receivers; (3) NOMA procedures, such as uplink transmission detection, link adaptation MA, synchronous and asynchronous operation, and adaptation between OMA and NOMA; (4) link and system level performance

evaluation or analysis for NOMA, such as traffic model and deployment scenarios of eMBB, mMTC and URLLC, coverage, latency, and signalling overhead.

1.4 Outline of the Thesis

➢ Chapter 2 provides the background study of power domain NOMA and different digital modulation techniques used in the experiment as well as simulation.

➢ Chapter 3 of the thesis deals with the performance analysis of power domain NOMA under different modulation techniques. The whole analysis is performed in simulation mode using MATLAB considering fixed power allocation and optimization power allocation techniques for both two- user and three-user PD-NOMA systems.

➢ In chapter 4, the real time implementation of PD-NOMA system using software defined radio (SDR) kits is described along with the system performance in both 2.4 GHz and 5 GHz range.

➢ Chapter 5 gives the conclusion that we have derived from the results, and includes the future scope of research.

Chapter 2   Background Study of Power Domain NOMA and Various Digital Modulation Techniques

2.1   Introduction

This chapter includes the basic concepts of Power Domain Non-Orthogonal Multiple Access Techniques (PD NOMA) along with some important issues and challenges regarding the implementation of PD-NOMA in real life application. As our thesis is centred around the simulation and real test bed experimentation of PD-NOMA under various digital modulation schemes, a brief theoretical background of different digital modulation techniques (BPSK, QPSK etc.) is provided in this chapter.

2.2   Basic Concepts of PD-NOMA

2.2.1   System Model Description
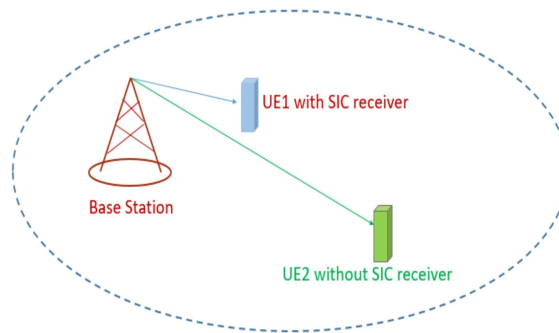
Fig.2.1. Downlink Power-Domain (PD) NOMA system model for two users

A simple PD-NOMA system model is presented in Fig.2. This system describes a single-cell downlink network scenario, where there is a single base station (BS)

and two user equipment (UE). User Equipment 1 (UE1) is nearer to the BS and thus, has a channel gain higher than that of UE2 (User Equipment 2), which is at the cell edge. The BS transmits superposed data of two users using Superposition Coding (SC) technique, where UE1 is allocated with α fraction of the total power, P_t, and UE2 is provided with (1-α) fraction of P_t. At the receiving end, UE1 performs successive interference cancellation (SIC) to remove UE2 data from the overall received signal, to extract its own data. As UE2 is provided with more power, it directly decodes its own signal without performing SIC.
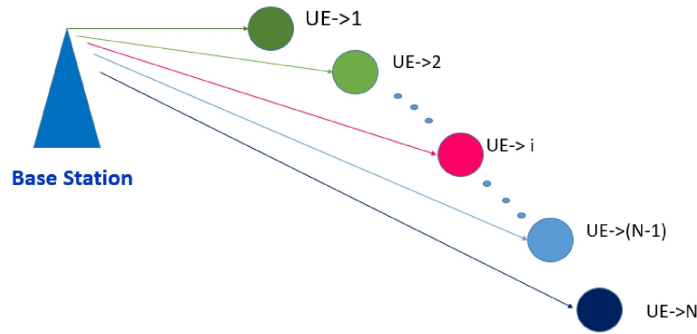
Fig.2.2. A typical PD-NOMA model with N users in downlink

A typical PD-NOMA scheme considers a single-cell downlink scenario with a single base station (BS) and N user equipments UE_i where $i \in N = \{1,2,\dots,N\}$ and all the user terminals are equipped with a single antenna. As seen in Fig. 2.2 UE_1 is in the smallest distance from BS whereas UE_N is in the largest distance from BS. Let us assume that total power transmitted from BS is P_t and the wireless links experience independent and identically distributed (i.i.d.) block Rayleigh Fading with AWGN. The channels are sorted as $0 > |h_1|^2 \geq |h_2|^2 \geq \dots \geq |h_{i-1}|^2 \geq |h_i|^2 \geq \dots \geq |h_{i+1}|^2 \geq |h_N|^2$ which indicates that UE_1 holds the strongest channels and has the prior information of the other channels for week users. At the BS signals from different users will be provided with different fraction of total power and then combined to transmit over same channel. The

strong user is given less fraction of power compare to the week one. So, the power allocation order is given as follows: $P_1 < P_2 < ... < P_{i-1} < P_i < P_{i+1} < ... < P_N$. At the receiver of UE_i SIC is performed. UE_i decodes and subtract the signals from UE_{i+1} to UE_N as those are weaker than UE_i itself and treats the signals from UE_{i-1} to UE_1 as interference as it cannot get rid of the signals from strong users.

2.2.2 Superposition Coding (SC)

In SC technique transmitter allows different users' signal to be superposed and transmitted through the same channel i.e., accessing same radio resources or same time-frequency resources. Transmitter performs encoding information regarding each user. For example, for a two-user scenario, the transmitter must to contain two point-to-point encoders that map their respective inputs to complex valued sequences of two users' signal. SC is recognized as a non-orthogonal scheme that achieves the capacity on a scalar Gaussian broadcast channel. In SC phase [24], two point-to-point encoders, $g_1 : \{0,1\}^{\lfloor 2^{TR_1} \rfloor} \to C^T$ and $g_2 : \{0,1\}^{\lfloor 2^{TR_2} \rfloor} \to C^T$ first map their respective input bits to two corresponding output bit sequences $S_1(n)$ and $S_2(n)$ and $\lfloor . \rfloor$ represents the floor operator where C is a code library. Then a summation device produces an output sequence as $X(n) = \sqrt{P_t \alpha_1}\, S_1(n) + \sqrt{P_t \alpha_2}\, S_2(n)$ where α_i represents a fraction of the total power P assigned to each user i ,subject to constrain $\alpha_1 + \alpha_2 = 1$.

2.2.3 Successive Interference Cancellation (SIC)

The fundamental idea behind SIC is that user signals are successively decoded. After one user's signal is decoded, it is deducted from the combined signal before decoding of the next user's signal. When SIC is employed, one of the user signals is decoded, considering the other user signal as an interferer, but the latter is then decoded with the benefit of the signal of the former having already been removed. However, prior to SIC, users are ordered according to their signal strengths in

such a manner that the receiver can decode the stronger signal first, subtract it from the combined signal, and isolate the weaker one from the residual part. In brief, the particular process involved in decoding the superposed messages can be mathematically expressed as follows [24]:

- ➤ At user 1, a single –user decoder $d_1: C^T \rightarrow \{0,1\}^{2^{TR_1}}$ decodes the message $S_1(n)$ by treating $S_2(n)$ as noise.

- ➤ User 2 performs the following steps to successively recover its message from its received signal $Y_2(n)$:
- ➤ Decode user 1's message $S_1(n)$ by using the single-user decoder $d_1: C^T \rightarrow \{0,1\}^{2^{TR_1}}$.

- ➤ Subtract $\sqrt{P\alpha_1}\ h_2 S_1(n)$ from the received signal $Y_2(n)$

$$Y_2'(n) = Y_2(n) - \sqrt{P\alpha_1}\ h_2 S_1(n) \dots \dots \dots (2.1)$$

Where, h_2 is the complex gain at user 2.

- ➤ Decode user 2's message $S_2(n)$ by using the single-user decoder $d_2: C^T \rightarrow \{0,1\}^{2^{TR_2}}$ on $Y_2'(n)$.

2.2.4   Mathematical Model

The general expression for the signal transmitted by the BS, in PD-NOMA system is given as follows [25]:

$$s(n) = \sum_{i=1}^{N} \sqrt{P_t \alpha_i}\ x_i(n) \qquad\qquad (2.2)$$

where, $x_i(n)$ is the information for the ith UE with unit energy; P_t is the overall transmission power at the BS; and α_i is the power coefficient allocated to the ith UE, subjected to the following condition:

$$\sum_{i=1}^{N} \alpha_i = 1 \qquad\qquad (2.3)$$

and $\alpha_1 \leq \alpha_2 \leq \ldots \leq \alpha_N$, since without loss of generality the channel gains have been assumed to be ordered as $|h_1|^2 \geq |h_2|^2 \geq \ldots \geq |h_N|^2$, wherein h_i is the channel coefficient of the ith UE, as per NOMA technique.

The general expression for received signal at the ith user equipment (UE) is as follows:

$$r_i(n) = s(n)h_i + w_i(n) \tag{2.4}$$

where, $w_i(n)$ is the zero mean complex additive Gaussian noise with a variance of σ_n^2.

The Signal to Interference-Noise Ratio (SINR) at the ith user equipment, except the 1st user equipment, can be expressed as follows:

$$SINR_i = \frac{\alpha_i \gamma |h_i|^2}{\gamma |h_i|^2 \sum_{k=1}^{i-1} \alpha_k + 1}, \forall i \neq 1 \tag{2.5}$$

The Signal to Interference-Noise Ratio (SINR) at the 1st user equipment is as follows:

$$SINR_1 = \alpha_1 \gamma |h_1|^2 \tag{2.6}$$

where, $\gamma = P_t / \sigma_n^2$, represents the transmit Signal to Noise Ratio (SNR).

The throughput of the ith user equipment in Downlink PD-NOMA system is given as follows:

$$R_i = B \log_2(1 + SINR_i) \tag{2.7}$$

where, B is the available transmission bandwidth.

Thus, the Sum Capacity of Downlink PD-NOMA system can be expressed as follows:

$$R_S = \sum_{i=1}^{N} R_i \tag{2.8}$$

2.3   Implementation Issues of NOMA

Practical implementation challenges regarding NOMA are considered in some studies. Some of those issues are mentioned below [25]:

Hardware Complexity: On comparison with Orthogonal Multiple Access (OMA), the complexity on the hardware side gets increased due to SIC implementation in NOMA. To obtain the lower power users' symbols, high power symbols are required to be estimated first with the SIC detector. If the number of users especially is high or fast signal transmission is required, the SIC procedure that is used multiple times, in addition to the detection delay, could cause important limitations for battery-limited devices. Since longer battery life is desired in consumer electronics, implementation of NOMA, particularly in dense networks, could be inefficient. This issue may limit usage of NOMA. To mitigate this problem effective user clustering and power allocation are become very crucial.

Error Propagation in SIC Implementation: According to the basic principle of NOMA, on the receiver side, SIC detection is employed to estimate the user with better channel condition first. Thus, the successful reception of the original signal depends on successful estimation of the high power signals. Since channel and hardware impairments are essential in the reception process, SIC detection can be negatively affected. Due to the presence of carrier frequency offset (CFO), timing offset (TO), and other hardware related impairments, it is complicated for NOMA systems to ideally estimate channel. So, erroneous detection and error propagation are there most likely to happen in the SIC detection method. To overcome this situation and to improve the transmission quality of the overall system, there is a necessity to opt for more robust way out. Instead of changing the main detector components, improvement over the estimation quality of

mentioned impairments is a more beneficial approach to obtain a practical performance gain of a system.

Optimal Pilot Allocation: According to the superposition coding principle multiple signals are transmitted in an overlapped fashion, due to which interference turns out and error performance causes degradation in NOMA, when compared to OMA systems. To obtain a good system performance it is an obvious fact to incorporate perfect or near-perfect Channel State Information (CSI). Pilot positions and the number of allocated pilots are precious design criteria in NOMA implementation. These are critical problems even in OMA systems due to undetermined channel characteristics in wireless communication environments. However, because of the inherent interference, optimal pilot allocation is more critical for NOMA systems and careful design is recommended. Therefore, channel characteristics should be tracked efficiently and accurately to distribute sufficient number of pilots at proper positions, which could result in good error performance in NOMA systems.

Instantaneous CSI Requirement: A serious problem occurs when a secondary user is provided a previously allocated frequency band; hence Channel State Information (CSI) for the transmission of this user should be determined with orthogonal transmissions. Due to this, an inexorable block of the main user signal transmission may arise an unfavourable situation. There is no clear proclamation whether this issue can be tolerated or not in real-time. Moreover, in dense networks, since there may be a requirement of instantaneous band allocation, this issue may become more severe. Effective and practical solution to this problem is very important for the future of NOMA systems. However, differences between the logics of these techniques should also be taken into account.

Carrier Frequency Offset and Timing Offset Estimation: Low-quality clocks used in wireless devices can cause significant occurrence of CFO and TO leading

to a noteworthy degradation in transmission quality. Utilizing the concept of multicarrier modulation technique used in OFDM renders robust CFO and TO estimation and provides the necessary correction. In the point-to-point OMA transmissions, joint estimation of CFO and TO is quite simple due to distinguishable received signals. Highly accurate synchronization support to devices can mitigate such disturbances; however, lower cost expectations may prevent such solution. Therefore, particularly, in uplink transmissions, distinguishability of overlapped signals should be obtained.

2.4   Digital Modulation Techniques - A Brief Discussion

Apart from modern mobile communication systems digital modulation techniques are used in the field of VLSI and DSP technology. The main advantages of digital modulation over analog modulation are greater noise immunity and robustness to channel impairments, easier multiplexing of various forms of information (e.g., voice, data and video), and greater security [26]. In addition to this digital signal transmission supports digital error control codes to detect or correct transmission errors and also responsive to source coding, encryption, and equalization to improve the performance of the overall communication link. A desirable modulation scheme provides low bit error rates at low received signal-to-noise ratio, performs well in multipath and fading conditions, occupies a minimum bandwidth, and is easy and cost effective to implement [26]. A brief description of linear digital modulation techniques (BPSK, QPSK) used in our thesis work is provided under this subtopic.

2.4.1 Binary Phase Shift Keying (BPSK)

In binary phase shift keying, the phase of a constant amplitude carrier signal is swapped between two values according to the two possible signals m_1 and m_2 corresponding to binary 1 and 0, respectively [26]. Generally, the two phases are

separated by 180°. If the sinusoidal carrier having an amplitude A_c and energy per bit $E_b = \frac{1}{2} A_c^2 T_b$, where T_b is the bit duration, then the transmitted BPSK signal is either

$$s_{BPSK}(t) = \sqrt{\frac{2E_b}{T_b}} \cos(2\pi f_c t + \theta_c) \qquad 0 \le t \le T_b \quad (binary\ 1) \qquad (2.9)$$

or

$$s_{BPSK}(t) = \sqrt{\frac{2E_b}{T_b}} \cos(2\pi f_c t + \pi + \theta_c)$$

$$= -\sqrt{\frac{2E_b}{T_b}} \cos(2\pi f_c t + \theta_c) \quad 0 \le t \le T_b \quad (binary\ 0) \qquad (2.10)$$

It is often suitable to generalize m_1 and m_2 as binary signal $m(t)$, which takes on one of two possible pulse shapes. Then the transmitted signal is represented as

$$s_{BPSK}(t) = m(t) \sqrt{\frac{2E_b}{T_b}} \cos(2\pi f_c t + \theta_c) \qquad (2.11)$$

The BPSK signal is equivalent to a double sideband suppressed carrier amplitude modulation waveform, where $\cos(2\pi f_c t)$ is employed as the carrier, and the data signal $m(t)$ is treated as the modulation waveform. Hence a BPSK signal can be generated with the help of a balanced modulator. The probability of bit error in BPSK considering an AWGN channel is found as,

$$P_{e,BPSK} = Q\left(\sqrt{\frac{2E_b}{N_0}}\right) \qquad (2.12)$$

2.4.2   Quadrature Phase Shift Keying (QPSK)

As two bits are transmitted in a single modulation symbol, Quadrature Phase Shift Keying (QPSK) has twice the bandwidth efficiency of BPSK. The phase of the carrier takes on one of the four equally spaced values, such as $0, \pi/2, \pi \ and \ 3\pi/2$,where each value of phase is represented by unique pair of message bits. The QPSK signal for this set of symbol states may be defined as

$$S_{QPSK}(t) = \sqrt{\frac{2E_s}{T_s}} \cos\left(2\pi f_c t + (i-1)\frac{\pi}{2}\right) \qquad 0 \leq t \leq T_s \quad i = 1,2,3,4 \qquad (2.13)$$

Where T_s is the symbol duration and is equal to twice the bit period.

The above equations can be rewritten for the interval $0 \leq t \leq T_s$ as

$$S_{QPSK}(t) = \sqrt{\frac{2E_s}{T_s}} \cos\left((i-1)\frac{\pi}{2}\right) \ \cos(2\pi f_c t)$$

$$- \sqrt{\frac{2E_s}{T_s}} \sin\left((i-1)\frac{\pi}{2}\right) \ \sin(2\pi f_c t)$$

$$(2.13)$$

Let us consider the two basis functions for the QPSK signal set over the interval $0 \leq t \leq T_s$ as

$$\emptyset_1 = \sqrt{\frac{2}{T_s}} \cos(2\pi f_c t) \ \ and \ \ \emptyset_2 = \sqrt{\frac{2}{T_s}} \sin(2\pi f_c t) \qquad (2.14)$$

The four signals can be expressed in terms of basis function as follows:

$$S_{QPSK}(t) = \left\{ \sqrt{E_s} \cos\left((i-1)\frac{\pi}{2}\right) \ \emptyset_1(t) - \sqrt{E_s} \sin\left((i-1)\frac{\pi}{2}\right) \ \emptyset_2(t) \right\}$$

$$(2.15)$$

The average probability of bit error in QPSK considering an AWGN channel is found as

$$P_{e,QPSK} = Q\left(\sqrt{\frac{2E_b}{N_0}}\right) \qquad (2.16)$$

It is a noticeable result that the bit error probability of QPSK is identical to that of BPSK, but twice as much data can be sent in the same bandwidth. Hence when we make a comparison between BPSK and QPSK, the later one provides twice the spectral efficiency with exactly the same energy efficiency.

Chapter 3   Performance Analysis of Power Domain NOMA under Different Modulation Techniques

3.1 Introduction

This chapter provides the detail performance analysis with respect to system bit error rate (BER) and sum capacity of downlink PD-NOMA system considering both two-user and three-user model. An optimum power allocation technique is introduced using constrained optimization algorithm to distribute power among users judiciously. The whole analysis is considered under different modulation schemes to showcase the effect on system BER of PD-NOMA system.

3.2 System model

This section highlights the underlying system models used in simulation through Fig.2.1 and Fig.3.1 where we considered downlink transmission separately for two-users as well as three-users. Equations (2.2) to (2.8) described in chapter 2 are used to build the mathematical model of PD-NOMA system. The simulation is performed using MATLAB software considering the effect of Rayleigh fading channel. As distribution of power among user equipment (UE) is very crucial challenge in PD-NOMA, a power allocation strategy is adopted in this thesis using constrained optimization technique.
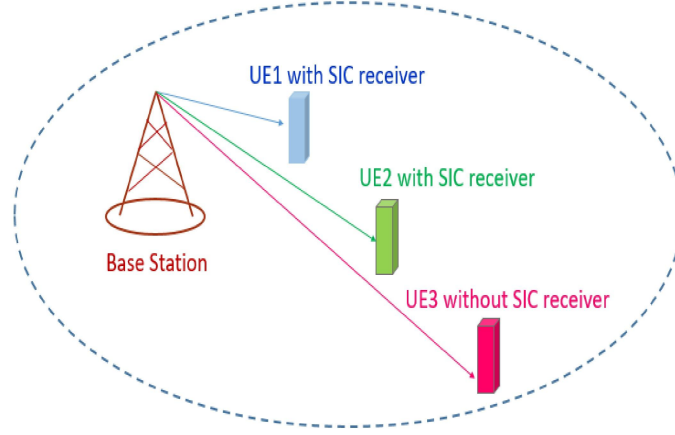
Fig.3.1. Downlink Power-Domain (PD) NOMA system model for three users

➤ *Power Allocation Using Constrained Optimization*

The goal of the Power Allocation (PA) mechanism is to maximize the sum capacity under a fairness constraint for the PD-NOMA system. The fairness factor indicates how fairly the system capacity has been shared among the UEs [27]. The Fairness Factor (FF) is given by:

$$FF = \frac{(\sum R_i)^2}{N \sum R_i^2} \qquad (3.1)$$

The constrained optimization problem statement is defined as:

$$\text{maximize} \quad R_S = \sum_{i=1}^{N} R_i \ ,$$

subject to the following constraints:

$$\sum_{i=1}^{N} P_i \leq P_t \qquad (3.2)$$

$$P_i \geq 0, \forall i \qquad (3.3)$$

$$F \geq F_T \qquad (3.4)$$

where, F_T is the target Fairness Factor of the system.

The optimum power allocation coefficients α_i for each UE is obtained through an exhaustive and iterative search. The algorithm 1 which describes the technique for optimizing the power allocation coefficients is given in Table-3.1:

Table 3.1: Algorithm for Optimum Power Allocation

Initialization

Initialize power_coefficient_matrix including all possible values

set maximum_capacity to zero

*for i in **power_coefficient_matrix** do*

    calculate sum_capacity

    calculate fairness_factor

    if fairness_factor > target_fairness_factor

      if sum_capacity(i) >= maximum_capacity

        maximum_capacity = sum_capacity (i)

        set required_set to power_coefficient_matrix

      end if

    end if

end for

The parameters used for simulation in MATLAB considering both two – users and three-users downlink PD-NOMA model are enlisted below in Table 3.2 and Table 3.3 respectively.

Table 3.2: Simulation Parameters for the two-user downlink PD-NOMA simulation model

Parameters	Selected values
Transmitted power	5 Watt
Power allocation coefficient for near user in fixed power allocation technique (for BPSK, QPSK, ADAPTIVE)	0.3
Power allocation coefficient for user 2 (farthest user)	0.7
Target fairness factor	0.7 and 0.85
Bandwidth	1 MHz

Table 3.3: Simulation Parameters for the three-user downlink PD-NOMA simulation model

Parameters	Selected values
Transmitted power	5 Watt
Power allocation coefficient for user 1 (nearest to base station) in fixed power allocation technique	0.02
Power allocation coefficient for user 2 (middle user)	0.14
Power allocation coefficient for user 3 (farthest user)	0.84
Target fairness factor	0.7 and 0.85
Bandwidth	1 MHz

3.3   Performance analysis of simulation model

3.3.1   *Simulation Result Analysis of two – user PD-NOMA model*

In this section, we present an extensive simulation result of the system BER and Sum Capacity for two-user downlink PD-NOMA system; firstly, for fixed type of power allocation and secondly using constrained optimization. All the analysis

regarding system BER and Sum Capacity are made considering three types of modulation schemes, under Rayleigh fading channel as follows:

1. BPSK modulation scheme for both near and far user
2. QPSK modulation scheme for both near and far user
3. QPSK modulation for near user and BPSK for far user, i.e., an **Adaptive Modulation approach.**
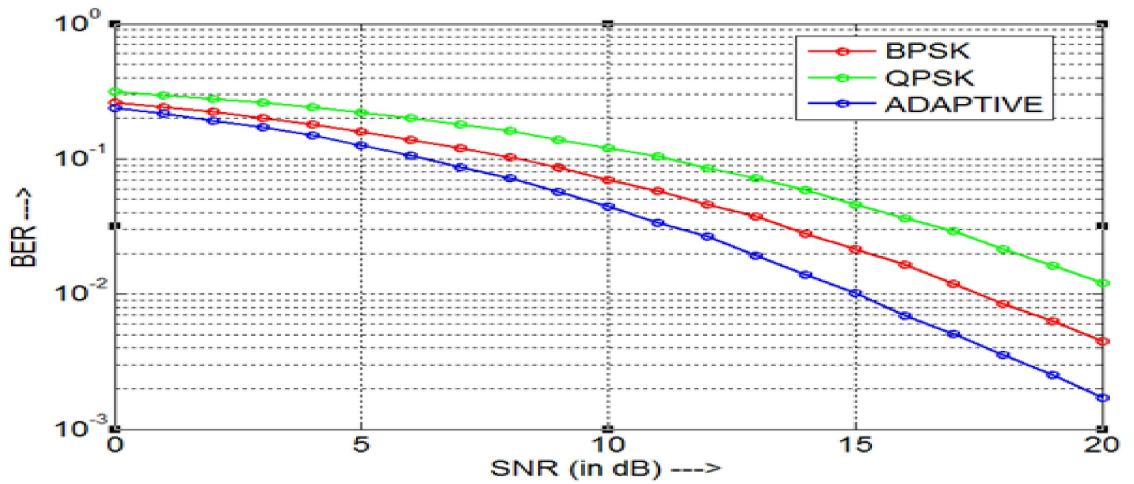
Fig.3.2. Comparison of two user PD-NOMA **System BER** plot for different Modulation Schemes using **Fixed Power Allocation Technique**
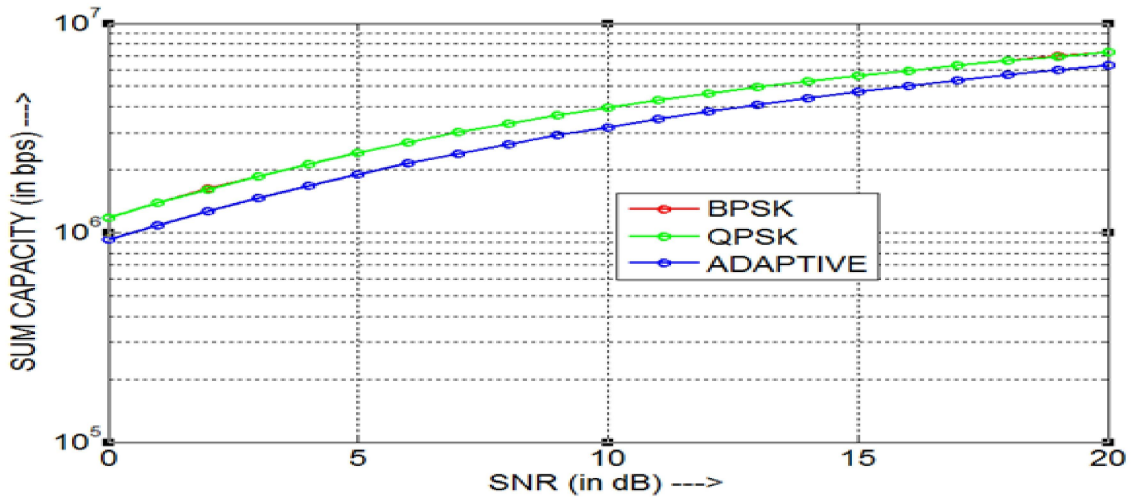
Fig.3.3. Comparison of **Sum Capacity** plot for different Modulation Schemes using **Fixed Power Allocation Technique**
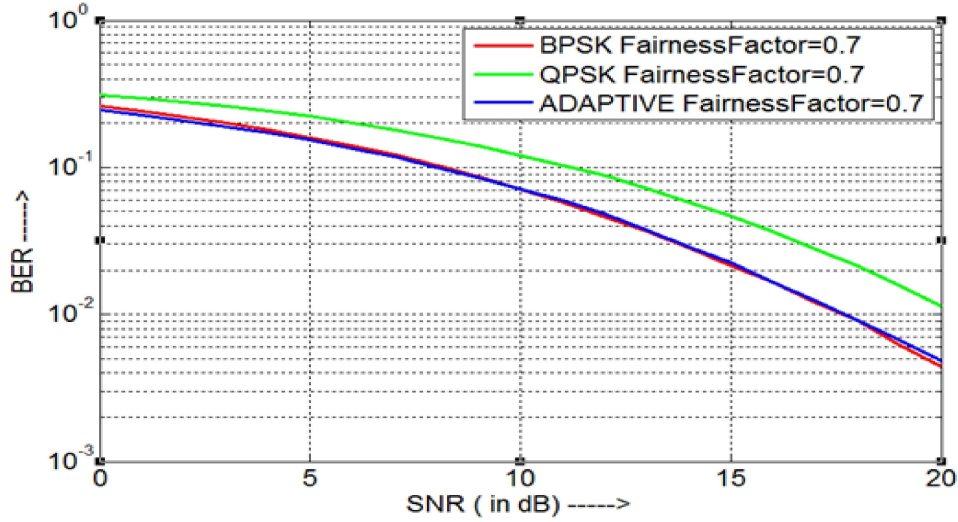
Fig.3.4. Comparison of **System BER** plot for different Modulation Schemes, using
Fairness Factor value = 0.7

Fig.3.2 shows the comparative analysis of system BER using the above mentioned modulation schemes in consideration with fixed power allocation to the UEs. For all the modulation techniques, a power coefficient of 0.3 has been assigned to the near UE, whereas a value of 0.7 has been allocated to the far UE. It is observed that the system BER for the adaptive modulation approach gives the lowest BER with respect to the range of transmit signal to noise ratio (SNR), i.e., 0 dB to 20 dB. However, when constrained optimization technique is employed for power allocation to the two UEs, it can be seen from Fig.3.4 & Fig.6, that both BPSK and Adaptive modulation techniques provide the same system BER plot. The reason behind this is that although the power coefficient set of [0.3 0.7] has been included in the initialization of power coefficient matrix, but as per the Constrained Optimization algorithm, only the set of power coefficient(s) that satisfy the necessary and sufficient conditions, is selected to be the optimum power coefficient for allocation to the UEs.
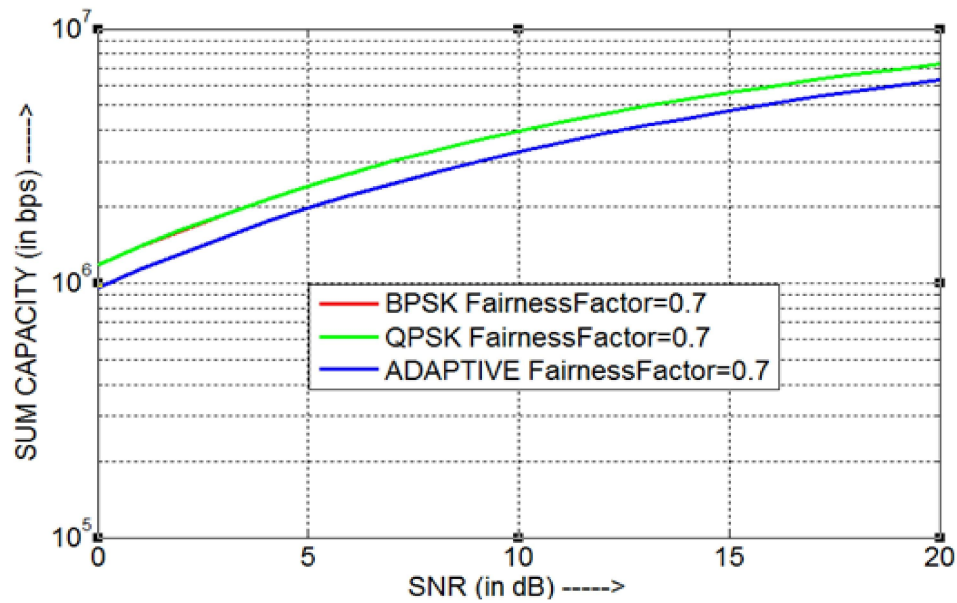
Fig.3.5. Comparison of **Sum Capacity** Plot for different Modulation Schemes, using
Fairness Factor value = 0.7
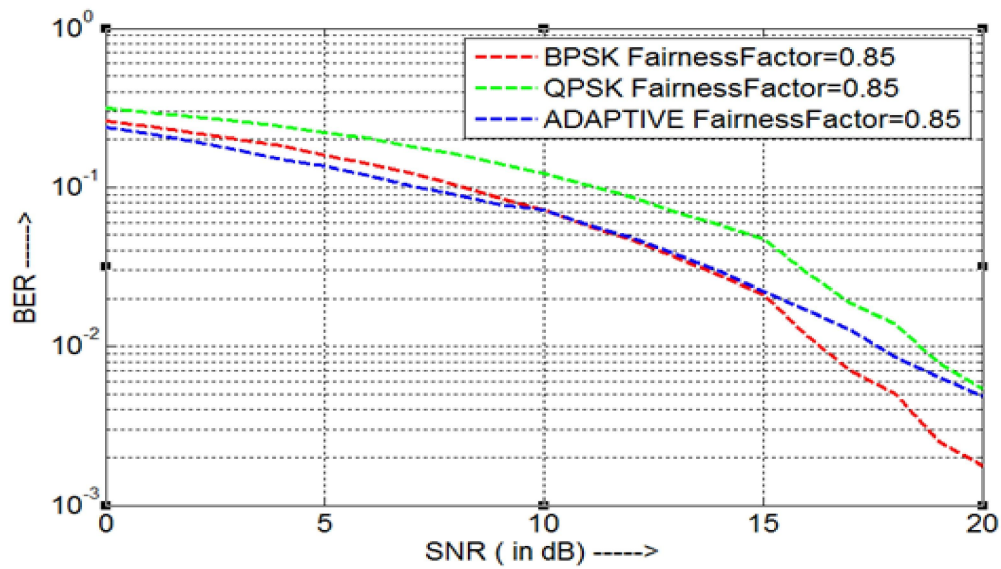
Fig.3.6. Comparison of **System BER** plot for different Modulation Schemes, using
Fairness Factor value = 0.85
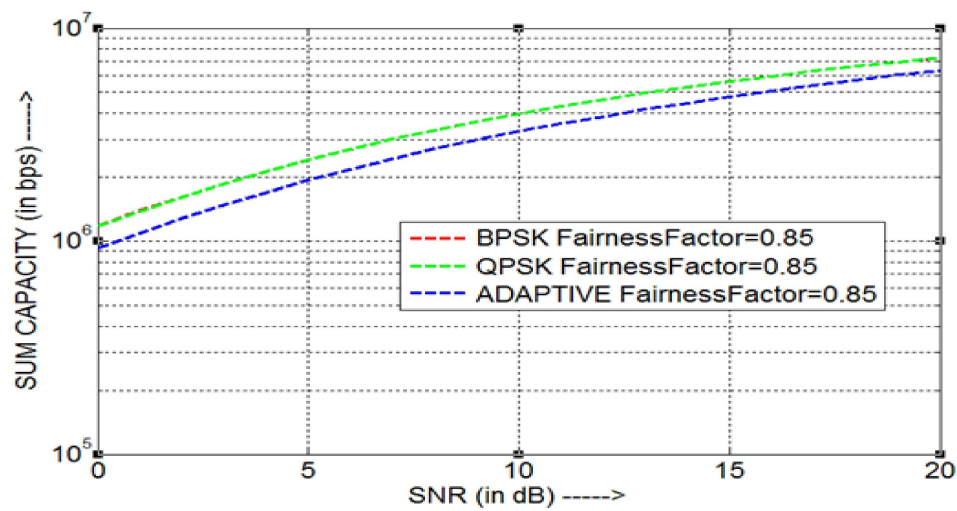
Fig.3.7. Comparison of **Sum Capacity** plot for different Modulation Schemes, using
Fairness Factor value = 0.85
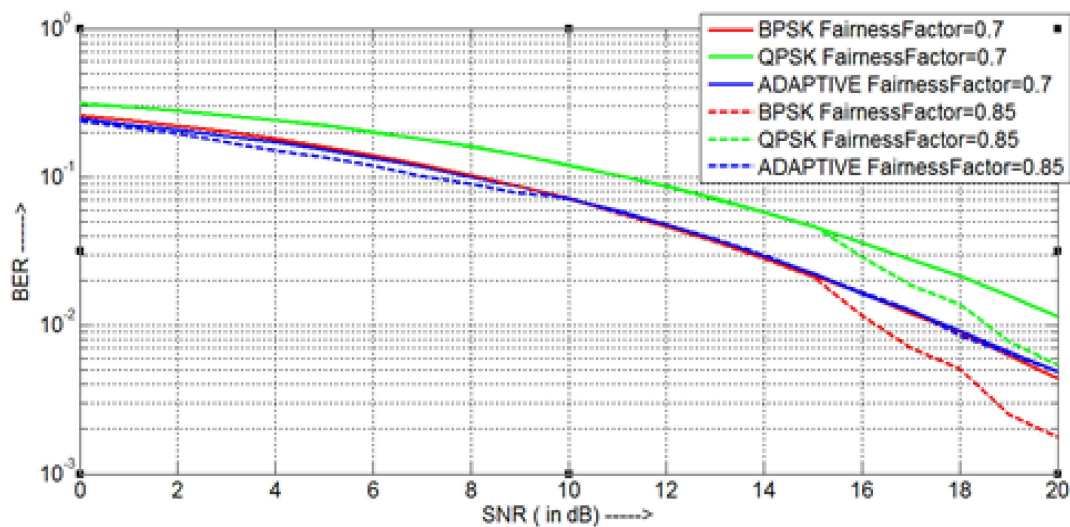
Fig.3.8. Comparison of **System BER** plot for different Modulation Schemes &
different **Fairness Factor values (0.7 & 0.85)**
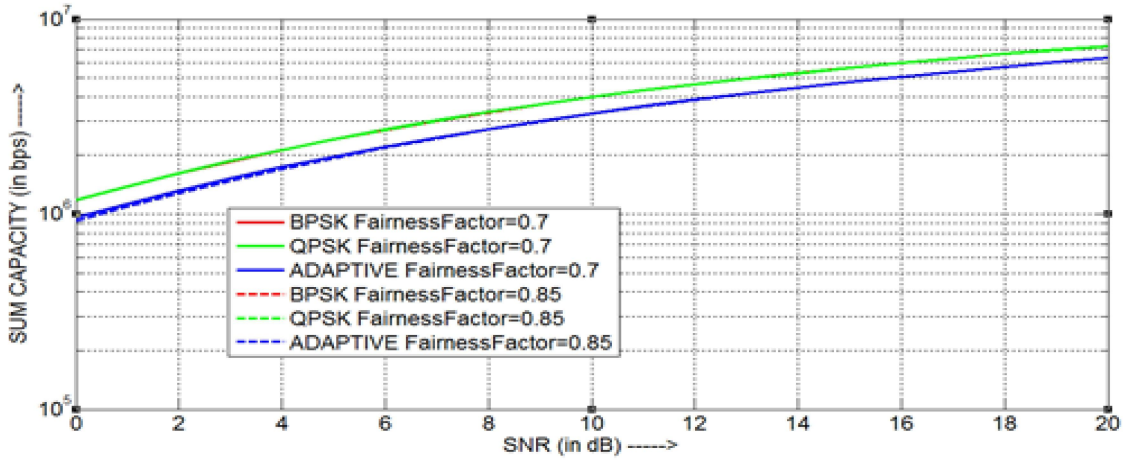
Fig.3.9. Comparison of **Sum Capacity** plot for different Modulation Schemes & **different Fairness Factor values (0.7 & 0.85)**

As conventional PD-NOMA adopts multiplexing users with different power allocations, the fairness level of achievable throughput of each user should be taken into consideration so that the throughput of those UEs approximately approaches to the same value. Hence, we have selected different target FF values, i.e., 0.7 & 0.85, to compare the respective system BER plots, given in Fig.3.4 & Fig.3.6, as well as the sum capacity plots, shown in Fig.3.5 & Fig. 3.7, for different modulation schemes using constrained optimization power allocation strategy.

It has been observed that when target FF is set to 0.7, the system BER plots for all the modulation schemes are smooth, as shown in Fig.3.4; because the system uses only one set of power coefficients for the entire range of transmit SNR. However, when the target FF is 0.85, the system BER plots for almost all the modulation schemes decrease, with increasing transmit SNR, in a step-like manner. This is because the algorithm dynamically assigns different sets of optimum power coefficients for different ranges of transmit SNR. Hence, it can be said that the FF does play a significant role in constrained power allocation technique.

Fig.3.8 provides a comparative analysis among the system BER plots of the various modulation schemes, including both the target fairness factor values of 0.7 and 0.85. The system BER plots of all the modulation schemes mostly follow their same respective paths, for both the values of target FF, because of similar allocation of power-coefficients by the optimization algorithm. However, for the transmit SNR range beyond 14dB, the system BER plots of both BPSK and QPSK, for target FF 0.85, drift away from that of target FF 0.7; since the optimization algorithm dynamically assigns different sets of power coefficients for different values of transmit SNR.

Fig.3.3 depicts the Sum Capacity plots of different modulation schemes using fixed power allocation technique. It is observed that the sum capacity plot of adaptive modulation technique is lower than that of BPSK and QPSK; and the sum capacities of both BPSK and QPSK are merged, indicating that although they might provide different throughput for different UEs but the overall sum rate is same since the power allocation coefficients are similar. The same pattern is followed in Fig.3.3 as well as Fig.3.5, which represent the sum capacities of different modulation schemes for the target FF values of 0.7 and 0.85, respectively, using constrained optimization algorithm.

Fig.3.9 presents a comparative analysis of sum capacities for different modulation schemes along with target fairness factor values of 0.7 and 0.85. It has been observed that despite increasing the value of target fairness factor from 0.7 to 0.85, the sum capacity plots of BPSK, QPSK as well as Adaptive modulation schemes follow the same trajectory for both the values of target FF. In both the cases, the sum capacities of BPSK and QPSK remain merged and above that of Adaptive modulation scheme. It is because if the power coefficient set allocated to the users are similar for different modulation schemes, then the sum capacity for those modulation techniques will also vary minutely. Hence, power allocation strategy plays a major role in PD-NOMA system.

3.3.2 Simulation Result Analysis of three – user PD-NOMA model

Likewise, the two – user model, this section presents an extensive simulation result of the system BER and Sum Capacity for three-user downlink PD-NOMA system for both fixed type of power allocation and using constrained optimization power allocation technique. All the analysis regarding system BER and Sum Capacity are made considering four types of modulation schemes, under Rayleigh fading channel as follows:

1. BPSK modulation scheme for all the three users

2. QPSK modulation scheme for all the three users

3. QPSK modulation for the nearest user (UE 1) and BPSK for the middle and far users (UE 2 and UE 3 respectively), i.e., an **Adaptive Modulation approach.**

4. Another **Adaptive Modulation approach** considering QPSK modulation for both the nearest user (UE 1) and middle one (UE 2) and BPSK for the farthest one i.e., UE 3.
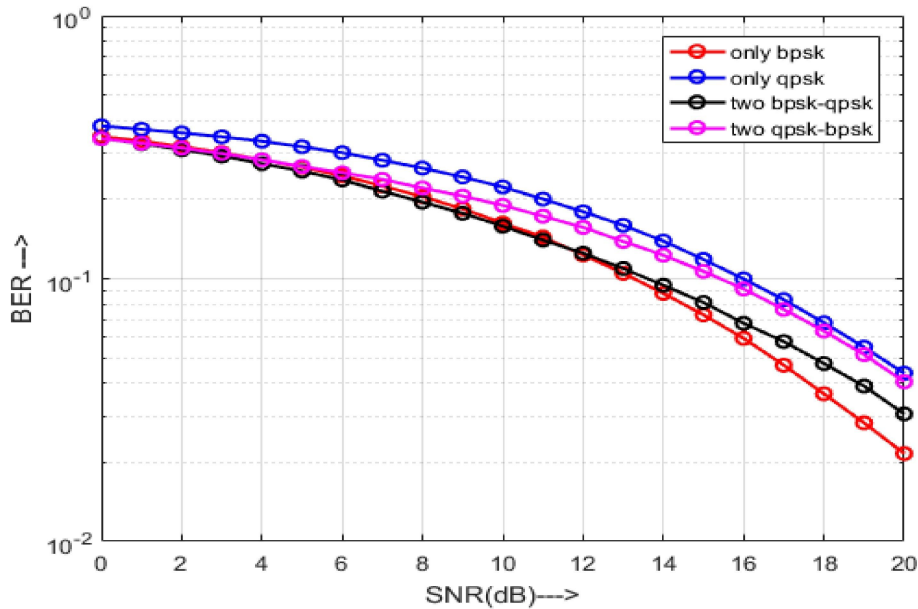
Fig.3.10. Comparison of three user PD-NOMA **System BER** plot for different Modulation Schemes using **Fixed Power Allocation Technique**
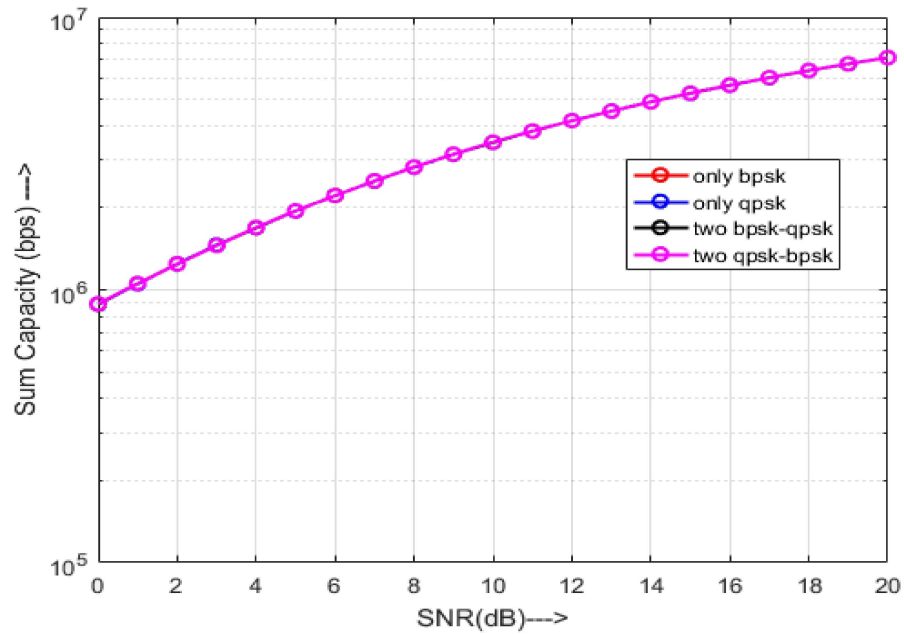
Fig.3.11. Comparison of **Sum Capacity** plot for different Modulation Schemes using **Fixed Power Allocation Technique in three user PD-NOMA model**
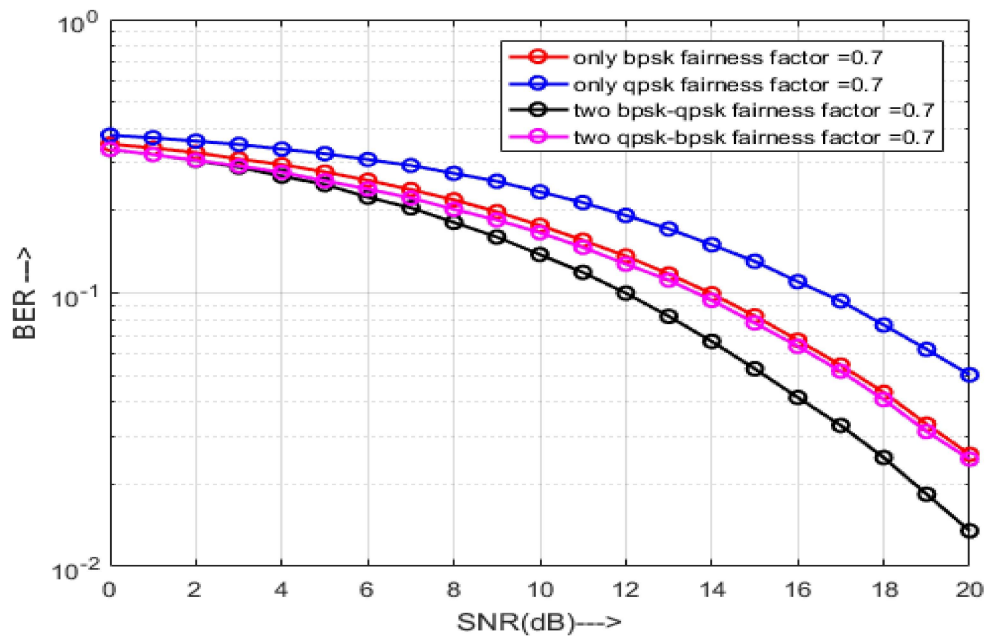
Fig.3.12. Comparison of three user PD-NOMA **System BER** plot for different Modulation Schemes, using **Fairness Factor value = 0.7**
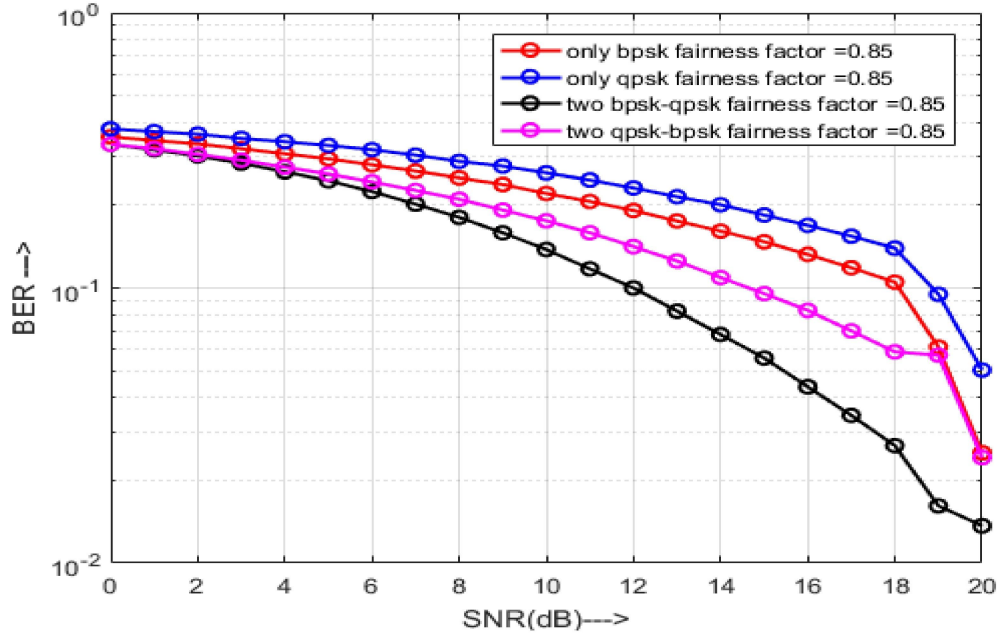
Fig.3.13. Comparison of three user PD-NOMA **System BER** plot for different
Modulation Schemes, using **Fairness Factor value = 0.85**
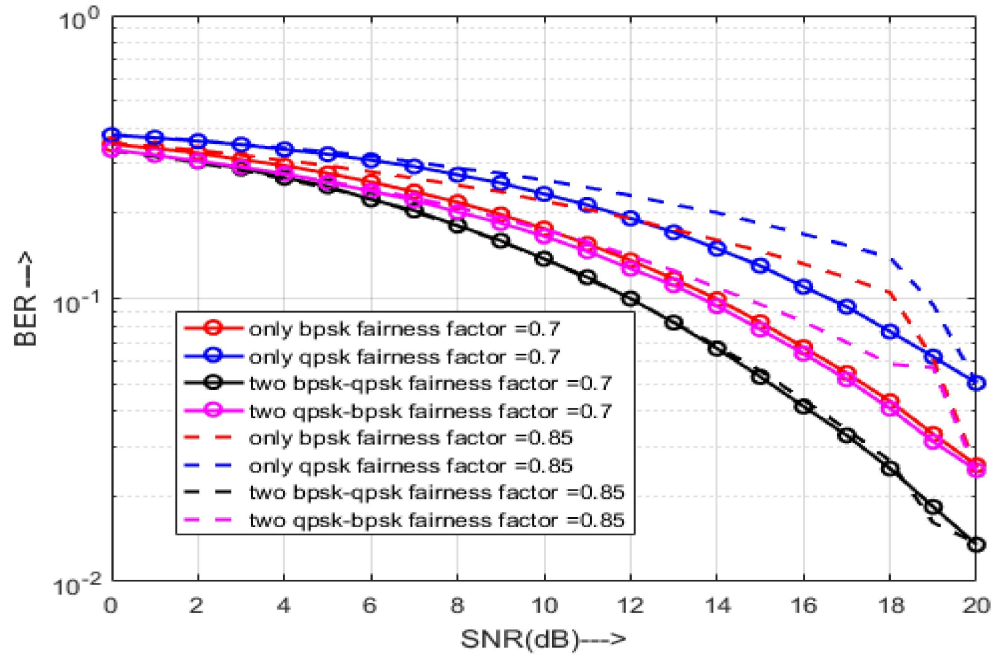
Fig.3.14. Comparison of three user PD-NOMA **System BER** plot for different
Modulation Schemes & different **Fairness Factor values (0.7 & 0.85)**

In Fig.3.10, a comparative system BER plot is provided with respect to transmit signal-to-noise ratio for the above mentioned four types of modulation schemes considering fixed power allocation to the three users. It has been observed that from 12 dB SNR onwards only BPSK modulation approach provides the lowest BER among other modulation techniques although all the BER curves follow the same trend of water falling curve with increasing transmit SNR. The sum capacity of the system for all kind of modulation approach are merged depicted in Fig.3.11 which indicates that although they might provide different throughput for different UEs but the overall sum rate is same due to the similar power allocation coefficients.

Fig.3.12 and 3.13 show that adaptive modulation technique, where middle user (UE2) and far user (UE3) are kept under BPSK modulation, provides the least BER with respect to transmit SNR while considering the constrained optimization power allocation technique. The step down falling of BER curve in Fig.3.13 can be explained as the optimization algorithm dynamically assigns different sets of optimum power coefficients for different ranges of transmit SNR.Fig.3.14 depicts comparison of three user PD-NOMA System BER plot for different modulation schemes & different Fairness Factor values (0.7 & 0.85).

Chapter 4   Real Time Implementation of PD NOMA using WARP: A Software Defined Radio Kits

4.1 Introduction

This chapter highlights the real testbed implementation of PD-NOMA using a software defined radio kit called Wireless Access Research Platform (WARP) transceiver system. The chapter starts with describing the detailed functionality of WARP boards followed by the design model of PD-NOMA OFDM system used in the experiment to produce a rigorous analysis of system performance with respect to system bit error rate under different modulation schemes. As NOMA is a promising solution to 5G technology, we have performed the experiment both in 2.4 GHz and 5GHz band.

4.2 Description of Wireless Access Research Platform

4.2.1 WARP: Introduction to a custom research platform

Wireless Open-Access Research Platform (WARP) is a well-recognized platform for research in advanced wireless algorithms and applications. It is a standard scalable and programmable wireless platform to model the prototype for advanced wireless networks. The platform architecture consists of four key components: custom hardware, platform support packages, open access repository and research applications; all together constituting a reconfigurable wireless testbed for students and faculty [27].

WARP is developed by the RICE University research team and distributed by Mango Communication. It is able to transmit in the range from 2.4 GHz to 2.5

GHz as well as up to 5.875 GHz range with 40 MHz bandwidth. The centre of the WARP node is positioned with a Xilinx FPGA board which provides all the processing resources of a node.

A number of other wireless testbeds and commercial products exist which provide some capabilities similar to WARP. For example, the GNU Radio project provides a flexible wireless development platform which includes an open-source framework of wireless algorithms implemented in software [28]. But with the bulk of the processing offloaded to a host PC, current GNU Radio systems cannot achieve the kind of high-throughput, wide-band communications provided by WARP. Commercial platforms, such as those from Sundance [29] and Lyrtech [30], provide some RF capabilities similar to WARP. However, these systems do not provide an open framework for algorithmic implementation at both the physical and MAC layers, a key provision of WARP.

- **Why to choose WARP as a wireless research tool**

WARP is asserted to be unique in its combination of high-performance programmable radio interfaces with open-access frameworks which enable wireless architecture, physical layer and network protocol research. WARP has become widely used in the research community due to its effectiveness in implementing various wireless protocols (e.g., 802.11 g/n PHY and MAC) and achieving real-time performance. It also supports MIMO since it has multiple RF interfaces. Hence, we have chosen to use it as our wireless research tool for real-time over-the-air transmission and reception.

4.2.2   WARP as a Software Defined Radio (SDR) Kit

Software-defined Radio (SDR) is a programmable transceiver kit which has a potential to operate on various wireless communication protocols without the necessity of changing or updating the associated hardware [31]. Software

Defined Radio (SDR) is promised to be designed for providing a cost effective and flexible solution by implementation of a wide variety of wireless protocols in software. The SDR has become increasingly well accepted in recent years due to its ability to realize many applications without a lot of effort in the integration of different components. This device allows engineers to include more features in the communication system and implement any number of different signal processing elements or protocols without changing the original system hardware and its architecture. It provides a customizable and portable communications platform for many applications, including the prototyping and realization of wireless protocols and their performances. It is also able to interface with a hardware module separately to communicate over a real channel.

Previous radio components, such as filters, modulation, demodulation, detectors, amplifiers, and mixers are used to implement the SDR in software for radio communication [32]. The motherboard is placed between the daughter board (RF front-end or TX RF) and host computer (software) at both transmitter and receiver. ADC/DAC is used to change the data format from analog to digital form and vice versa. Field Programmable Gate Array (FPGA) helps to execute high bandwidth mathematical calculations such as decimation, modulation/demodulation, digital down conversion, digital up conversion and interpolation processes. The wired Ethernet is there to transmit and receive data between motherboard and host computer [33].

The architecture of SDR at the receiver and transmitter are shown in the figure below.

Transmitter

Software → FPGA → Digital to Analog Converter DAC → Transmit RF → TX antenna

Receiver

Software ← FPGA ← Analog to Digital Converter ADC ← Receive RF ← RX antenna
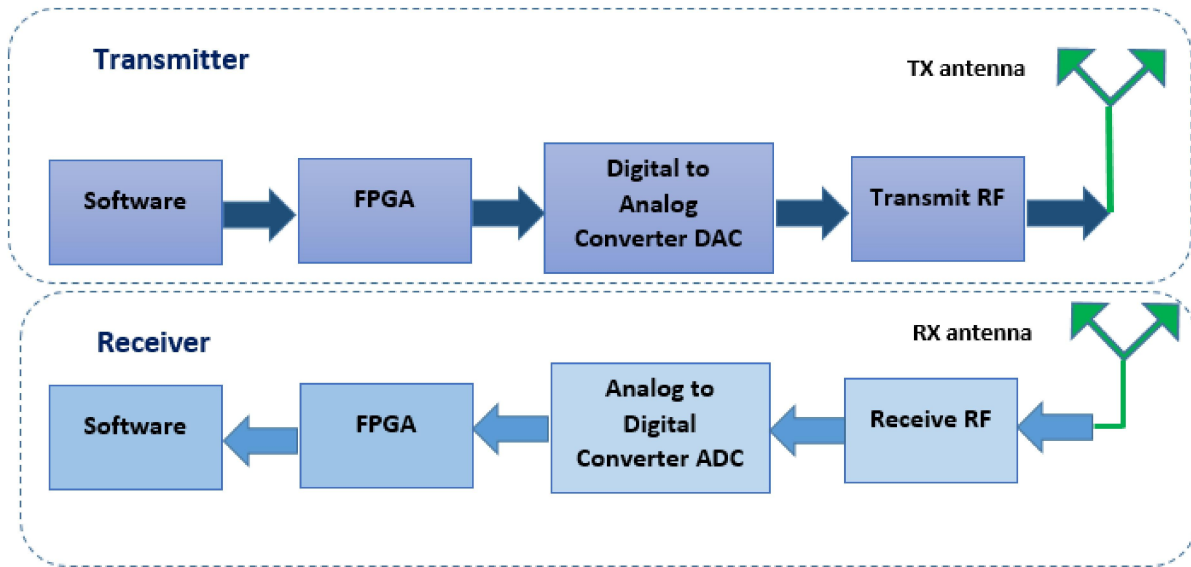
Fig.4.1. Basic SDR Architecture

The programmable hardware SDR has three approachable techniques, viz. digital signal processors (DSPs), Field Programmable Gate Arrays (FPGAs) and making use of a General Purpose Processor (GPP) in a regular computer [34]. WARP is the example of an SDR which is implemented on an FPGA hardware platform, and depends on the embedded processors on board.

An FPGA is an array of programmable logic blocks, such as general logic, memory, and multiplier blocks, surrounded by a programmable routing fabric. This circuit is capable of implementing any design or function, where updating of it becomes very easy. Multiple computational operations can be performed in parallel with the advantageous architecture of FPGA. Parallelism enables substantial data throughput at relatively low lock rates.

The latest version of WARP is equipped with a relatively powerful FPGA for signal processing. It also provides a higher processing capacity than software based SDR platforms.

4.2.3   WARP v3 kit

WARP v3 [33] is the latest generation of WARP hardware, integrating a high performance FPGA, two flexible RF interfaces and multiple peripherals to facilitate rapid prototyping of custom wireless designs. WARP v3 contains a

Xilinx Virtex-6 LX240T FPGA, which includes two Micro Blaze processors and a Gigabit Ethernet peripheral. It is able to achieve the high symbol rates while executing all the signal processing inside the FPGA.

The following block diagrams taken from WARP manual give an idea regarding the platform's modular and layered architecture where the hardware components are depicted.
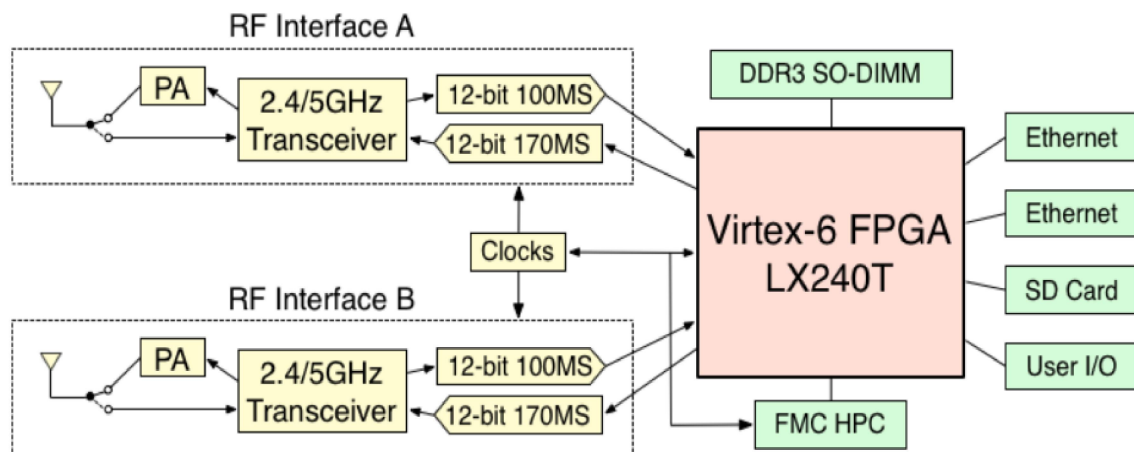
Fig.4.2. Block Diagram of WARPv3

Fig.4.3. Top view of WARPv3 (Unlabelled)
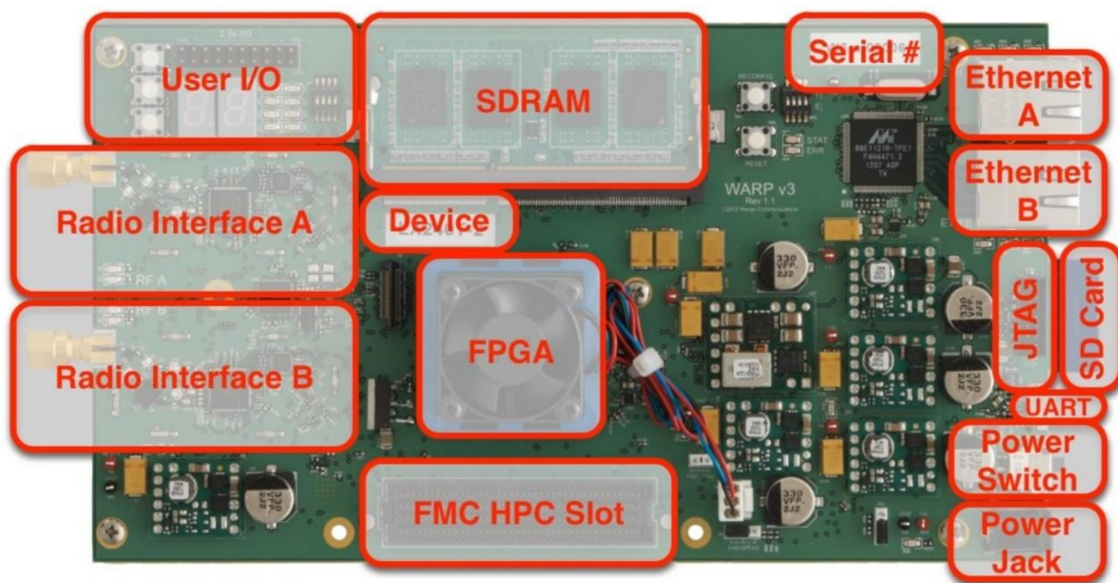
Fig.4.4. Top view of WARP v3 (Labelled)
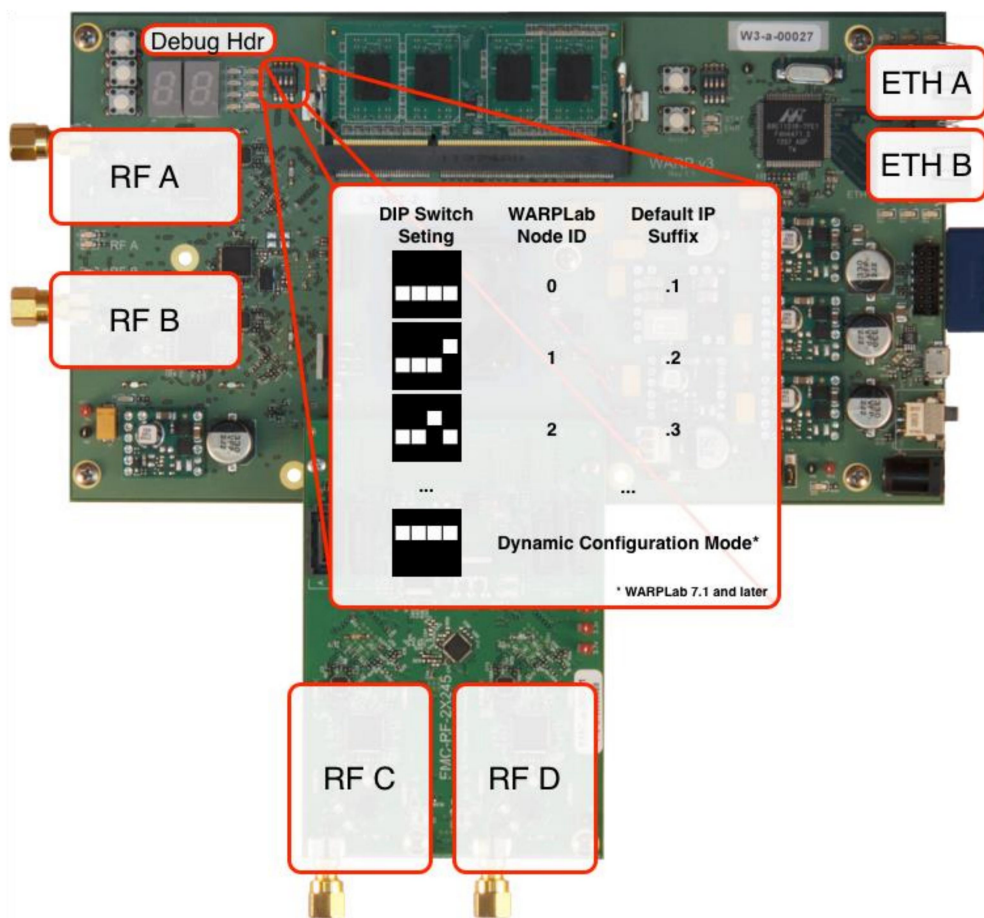
Fig.4.5. WARP v3 Board with FMC Connected

4.2.3.1 Key Components of WARP v3 Hardware

The following is a list of components [34] along with a high-level description of what each component is responsible for.

- **User I/O:** This collection of push buttons, LEDs, hexadecimal displays, dip switches, and debug header pins is used for interacting with the board. Designs can read values from the switches and push buttons and can write values to the displays and LEDs. The debug header can be used for any number of purposes, such as providing a convenient way for one WARP board to trigger the action of another board over a wire.

- **Radio Interfaces A & B:** These interfaces provide the radios that allow designs to communicate at the 2.4 GHz and 5 GHz bands. For each radio interface, digital I and Q values from the FPGA are taken through digital-to-analog converters and are delivered to the transceiver for up conversion (i.e., wireless transmission). Wireless reception follows the reciprocal process where I and Q analog streams are taken from the transceiver through analog-to-digital conversion and are then delivered to the FPGA. The interfaces are labelled "RF A" and "RF B" on the board and in the reference designs.

- **SDRAM:** This DDR3 SO-DIMM provides extra memory beyond the block RAM inside the FPGA. The WARP v3 kit ships with a pre-tested 2GB SO-DIMM.

- **Device label:** This label shows the FPGA device on the WARP v3 board. This device is used in a number of places during the development process (such as exporting a peripheral core from Xilinx System Generator), so this label is present for convenient lookup.

- **Virtex-6 FPGA:** Under the fan, the FPGA serves as the central processing system for the WARP board.

- **FMC HPC Slot:** The FPGA Mezzanine Card High Pin Count slot provides connectivity to an existing ecosystem of hardware as well as future WARP-specific modules.

- **Serial Number:** This is the unique serial number for the WARP board. This number is also programmed into an EEPROM on the board prior to shipping, allowing software running on the hardware to read this information.

- **Ethernet A/B:** The two 10/100/1000 Ethernet ports provide high-speed connectivity between the board and a wired network. The ports are labelled "ETH A" and "ETH B" on the WARP v3 board and in our reference designs.

- **JTAG:** The JTAG connector allows direct programming of the Virtex-6 FPGA using a Digilent or Xilinx JTAG cable.

- **SD Card:** An alternative to programming the board over JTAG is to use the SD card. This allows non-volatile storage of programs that will automatically download and execute upon insertion of the SD card.

- **UART:** The micro-USB connector on the board allows programs on the board to print messages to a terminal running on a computer.

- **Power Switch:** The power switch controls power to the board. The "off" position is where the switch is furthest away from the power jack. The "on" position is where the switch is closest to the power jack.

- **Power Jack:** The power jack is where the 12V power supply that comes with the WARP hardware should be plugged in. **Note: the power switch should be in the "off" position whenever the power plug is inserted or removed.** This allows the circuitry controlled by the switch to properly sequence the power regulators on the board.

The board resources for WARPv3 are tabulated below in table 4.1 [33]:

Table 4.1: Board Resources of WARP v3

Memory	● DDR3 SO-DIMM Slot
Ethernet	● Two Gigabit interfaces
Multi Gigabit Transceivers	● 2.4/5GHz transceiver (40MHz RF bandwidth) ● 12-bit 170 MSps DAcs, 12-bit 100MSps ADCs
MGT Clocking	● Dual-band PA (20 dBm, TX power) ● Shared Clocking MIMO applications
UART	● FMC HPC expansion slot
User I/O	● 2 Seven Segment Displays ● 12 LEDs ● 4 Push buttons ● 4 bit DIP switch ● USB-UART ● 16-bit 2.5v I/O header

4.2.3.2   Basic Design Structure of WARP v3

To develop custom applications on WARP requires using design tools from Xilinx. All WARP reference designs are built using the Xilinx Embedded Development Kit (EDK). The EDK enables construction of designs with both a processor, for running custom software, and custom hardware cores for real-time processing and connecting to off-chip hardware.

The EDK includes two primary tools:

- Xilinx Platform Studio (XPS): It integrates the hardware cores for a design, including the MicroBlaze processor, memory, peripherals and interfaces for off-chip hardware

- Xilinx Software Development Kit (SDK): It is a full suite of software compilation and debugging tools for the MicroBlaze processor

The basic structure of WARP reference designs is illustrated below [35].

The major components of this architecture are:

- **MicroBlaze soft processor:** The MicroBlaze is a processor core implemented in the FPGA fabric and is supplied by Xilinx as part of the EDK.

- **Memories:** The Virtex-6 FPGA includes a large number of "block RAMs", or internal RAM blocks which can be interconnected to form arbitrarily sized memory areas accessible to the MicroBlaze. These block RAMs are used for cache, instruction and data storage.

- **Processor bus:** A standard bus connects the MicroBlaze to each core in the system. Current reference designs use a bus called PLB; future designs will migrate to the newer AXI standard.

- **Peripheral cores:** A collection of peripheral cores composing every hardware design. Some are provided by Xilinx (like the UART and Ethernet MAC). We have designed others (like the WARP v3 user I/O and radio interface cores).

- **Off-chip resources:** These blocks represent the other hardware on WARP v3 besides the FPGA, like the radio interfaces, FTDI USB-UART transceiver and Marvell Ethernet PHYs.
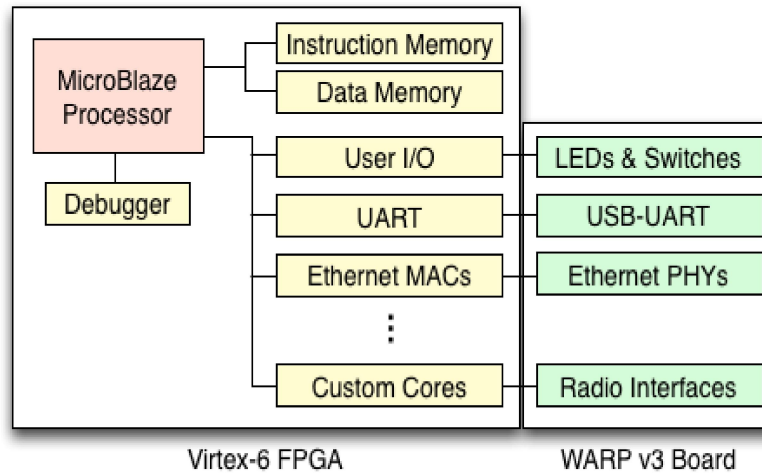
Fig.4.6. Basic Structure of WARP Reference Designs

The MicroBlaze processor and connected cores are all implemented in the FPGA fabric using XPS. The output of the XPS flow is a "bitstream" with the fully synthesized and implemented hardware design. This bitstream integrates the MicroBlaze, the standard peripheral cores, custom cores, I/O assignments and clock configurations. However, the MicroBlaze instruction and data memories are blank in this bitstream.

The XPS-generated bitstream (and its associated hardware specification) is the starting point for an SDK project. The SDK compiles custom code for the MicroBlaze, along with drivers for the various cores included in the XPS hardware design. The output of this process is an "elf" file, the software binary ready for execution by the MicroBlaze. The elf binary is combined with the XPS-generated bitstream to program the FPGA with the final hardware and software design.

4.2.4. Integration of WARP SDR kit with WARPLab Framework

WARP can communicate with a host computer through Ethernet connections. Experiments were implemented using the WARPLab framework [36] which

allows rapid prototyping of physical layer algorithms by combining the ease of MATLAB with the capabilities of WARP. WARPLab is a framework for rapid physical layer prototyping that allows for coordination of arbitrary combinations of single and multi-antenna transmit and receive nodes. The extensible framework gives users the flexibility to develop and deploy large arrays of nodes to meet any application or research need.

The WARPLab reference design is an implementation of the WARPLab framework that allows many physical layer designs to be constructed and tested. The reference design combines MATLAB and FPGA implementations of the WARPLab framework modules that allow for easy extensibility and customization. While the reference design uses MATLAB to control nodes and perform signal processing, it also allows applications with strict latency requirements to move time critical processing into the FPGA.

The WARPLab framework provides the software necessary for easy interaction with the WARP nodes directly from the MATLAB workspace; the software consists of FPGA code and MATLAB m-code functions, which are all available in the WARP repository.

> *Hardware requirements:*

The version used was WARPLab 7, which supports WARP v3 hardware.

For the 2-radio WARPLab reference design:

- WARP v3 nodes use the integrated RF interfaces

For the 4-radio WARPLab reference design:

- WARP v3 nodes must be equipped with the FMC-RF-2X245 radio FMC module

➢ *Software requirements:*

    ● MATLAB 2011a or later (Used in experiment: MATLAB 2014a)

➢ *Baseband Buffers Module Implementation*

The WARPLab Reference Design implements a Baseband module that buffers incoming and outgoing samples from radio interfaces. It supports up to 4 interfaces, including both I/Q and RSSI. On WARP v3 hardware, each buffer can be over 2^{15} samples long.

Two WARP boards were used, one as a transmitter node and the other one as the receiver node. The FMC-RF2X245 module dual-radio FPGA Mezzanine Card (FMC) daughterboard extends the capability of WARP v3 boards from 2 to 4 RF chains.

The experiments were implemented using the basic WARPLab setup where two WARP nodes are connected to a host PC via an Ethernet switch. This is illustrated in the figure below.
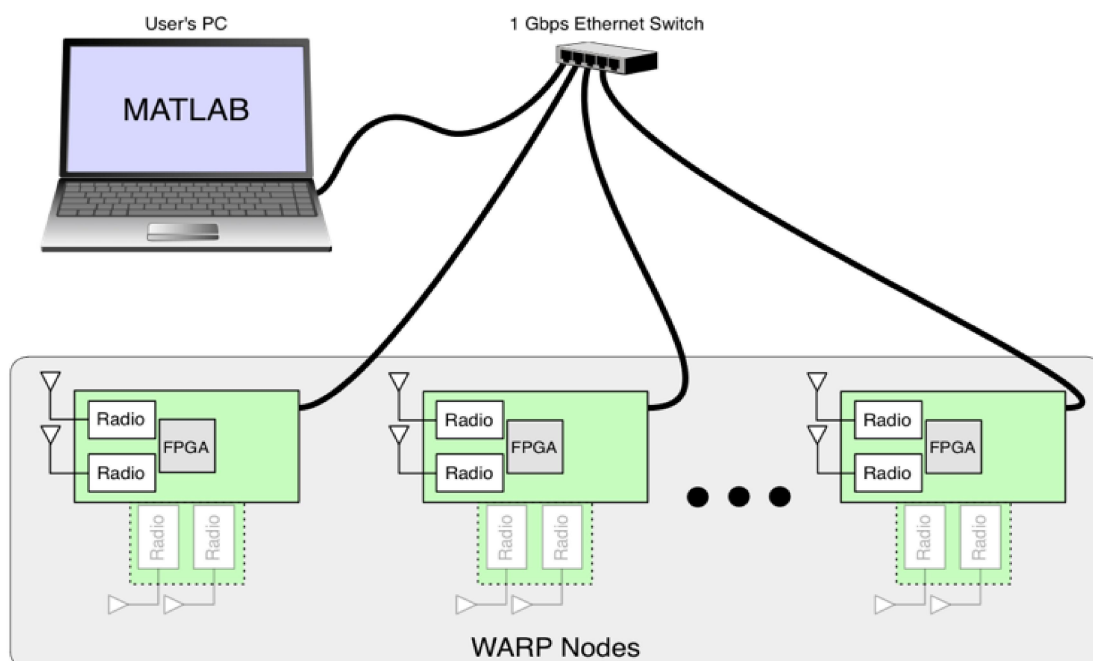
Fig.4.7. Example Set-Up

4.3 Design Model
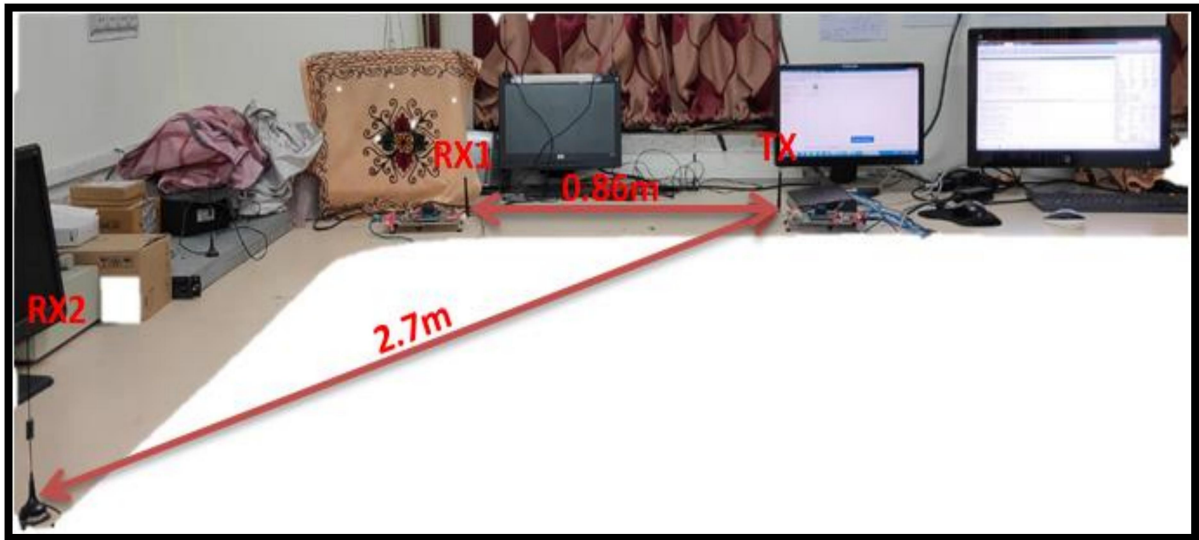
Fig.4.8. Experimental set up for two users downlink PD NOMA model

Fig.4.8 depicts the test-bed for PD-NOMA implementation for two-users using WARP kit and other necessary software. As it can be seen, one of the two WARP transreceiver boards has been set-up as the transmitting BS (TX) with a single antenna, while the other is configured as a receiver with two antennae; where each antenna is assigned to two separate users (RX1 & RX2) respectively. The number of receiver antenna can be expanded depending on the number of users involved in the system. As we are dealing with two users, hence we use only two antennae at the receiver board to avoid other experimental overhead complexity. Likewise, the number of transmitting antenna can also be increased as per design of the experimental model. The antennas of the receiver board are placed at considerable distance apart from each other so as to ascertain the concept of PD-NOMA, wherein suitable power allocation technique is applied depending upon the respective distance of the users from the BS. In our experiment, user 1, denoted by RX1, is the "near user" as it is at a distance of 0.86m from the BS, whereas user 2, denoted by RX2, will be regarded as the "far user" as it has been

placed at a distance of 2.7m from the BS. The distance of the users can be selected arbitrarily, as the designed model works for all possible situations. Although fixed power allocation technique is used in this experiment, the exhaustive analysis of system BER with respect to the near user's power allocation coefficient (α) leads us to select different sets of power coefficient values for different modulation schemes employed in the system. The values of α considered for BPSK, QPSK and Adaptive modulation techniques are 0.15, 0.27 and 0.4 respectively.

Fig.4.9. Experimental set up for three users downlink PD NOMA model

Fig.4.9 shows the experimental set up for PD NOMA model with three users.

The receiver WARP board is equipped with three antennas which represents three User Equipments (UEs) situated at three different distant places from the transmitter WARP board (in our case base station). UE 1 which is placed at a distance of 0.85m from BS is indicated as the nearest user. UE2 and UE3, which are located at distances 1.5m and 2m, are referred to as middle and far user respectively. The analysis of system BER is performed within the limited range

of transmit power (-33dBm to -19dBm) measured at RF port of WARP transmitter board. All the measurements have been carried out on Channel ID 1 having center frequency 2.412 GHz in the 2.4 GHz range.

4.4 Steps of Experimental Set-Up

- The power jack is plugged into the WARP v3 board with the test port, and the power switch is shifted to the "ON" position. If the FMC is to be connected to use a 4 RF Node configuration, it should be done first.

- JTAG cable is connected between the board's JTAG connector and the CPU of PC-1.

- The Xilinx iMPACT application is opened on PC-1. The IMPACT software application supports communication (including FPGA configuration) between a computer running IMPACT and devices on the WARP FPGA board configured in a "scan chain" [39]. In such a chain, serial data is fed from the output of each device to the input of its nearest downstream neighbour. The first and last devices in the chain are connected back to the PC via dedicated USB boundary scan circuitry on the WARP FPGA board. Establishing communication via this link is a critical first step in utilizing the WARP hardware.

- The basic communication link between the PC and the WARP FPGA board, made by Ethernet cables via a LAN switch, is used to configure the FPGA device (download a program to it). After a right-click on the FPGA icon, **Initialize Chain** [40] is chosen.

- In the 2 RF Node configuration (i.e., only RF A and RF B are populated), only the **2RF bitstream** should be used and in the 4 RF Node configuration (i.e., all RF interfaces are populated), the **4RF bitstream** should be used to program the FPGA board.

- After a right-click on the FPGA icon, **Program** is chosen.

- IMPACT is closed, leaving the board's Main Power switch in the ON state the USB cable connected.
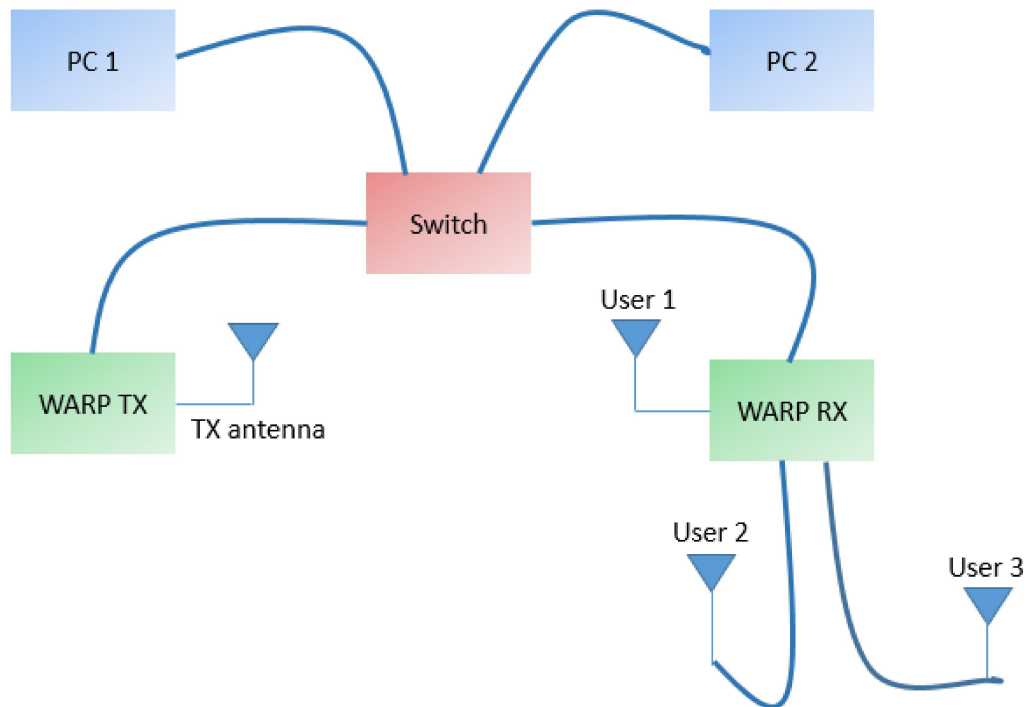
Fig.4.10. Block diagram of experimental set up for three-user downlink PD NOMA
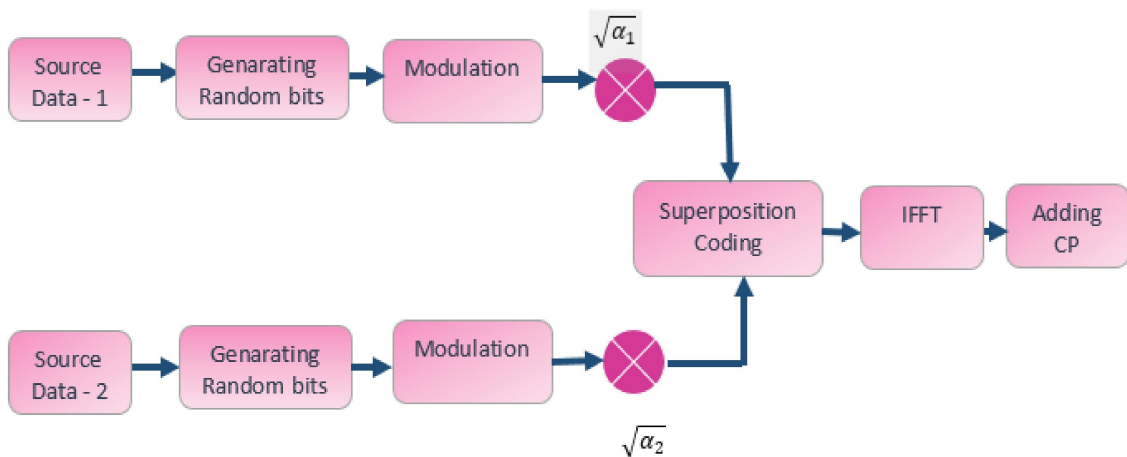
Fig.4.11. Block diagram of two-user downlink PD NOMA-OFDM based transmitter
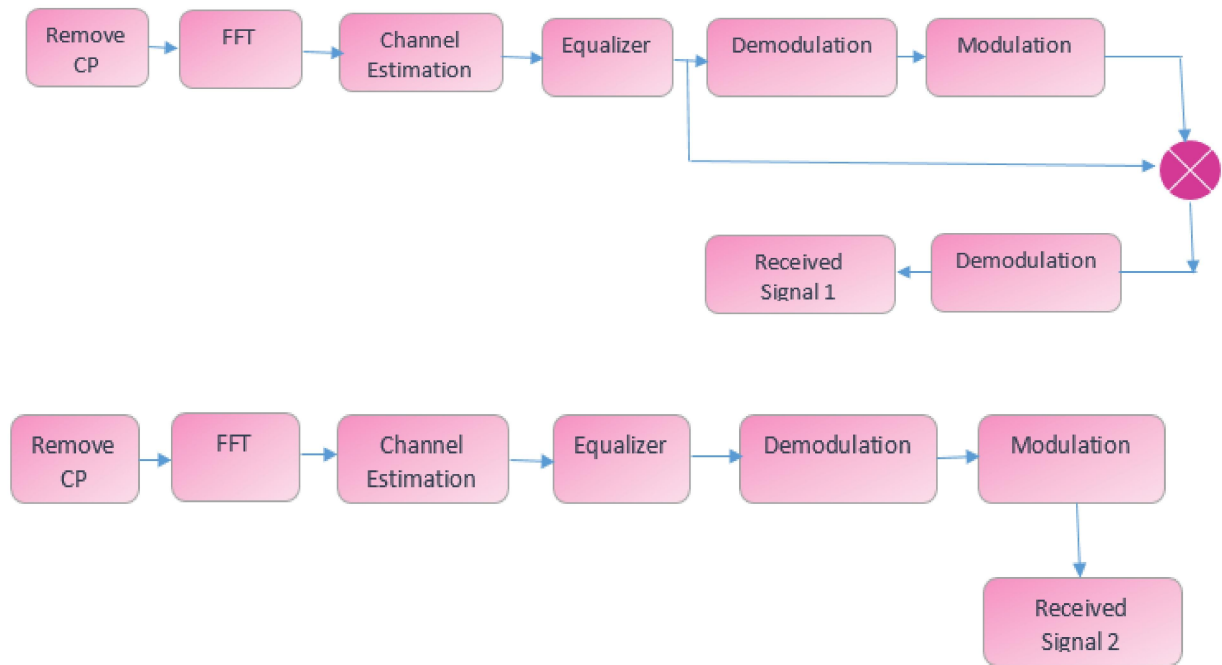
Fig.4.12. Block diagram of two-user downlink PD NOMA-OFDM based receiver

We have performed the PD-NOMA experiment considering two Single Input Single Output (SISO) configurations mentioned as follows:

1. WARP Tx node (RF port A) to WARP Rx node (RF port A) for near user
2. WARP Tx node (RF port A) to WARP Rx node (RF port B) for far user

The three-user PD-NOMA model is considered with three SISO configurations mentioned below:

1. WARP Tx node (RF port A) to WARP Rx node (RF port A) for near user
2. WARP Tx node (RF port A) to WARP Rx node (RF port B) for middle user
3. WARP Tx node (RF port A) to WARP Rx node (RF port C) for far user

4.5 OFDM System Design

The block diagram implementation of OFDM technique for 1x1 SISO configuration on the WARP module is shown below:
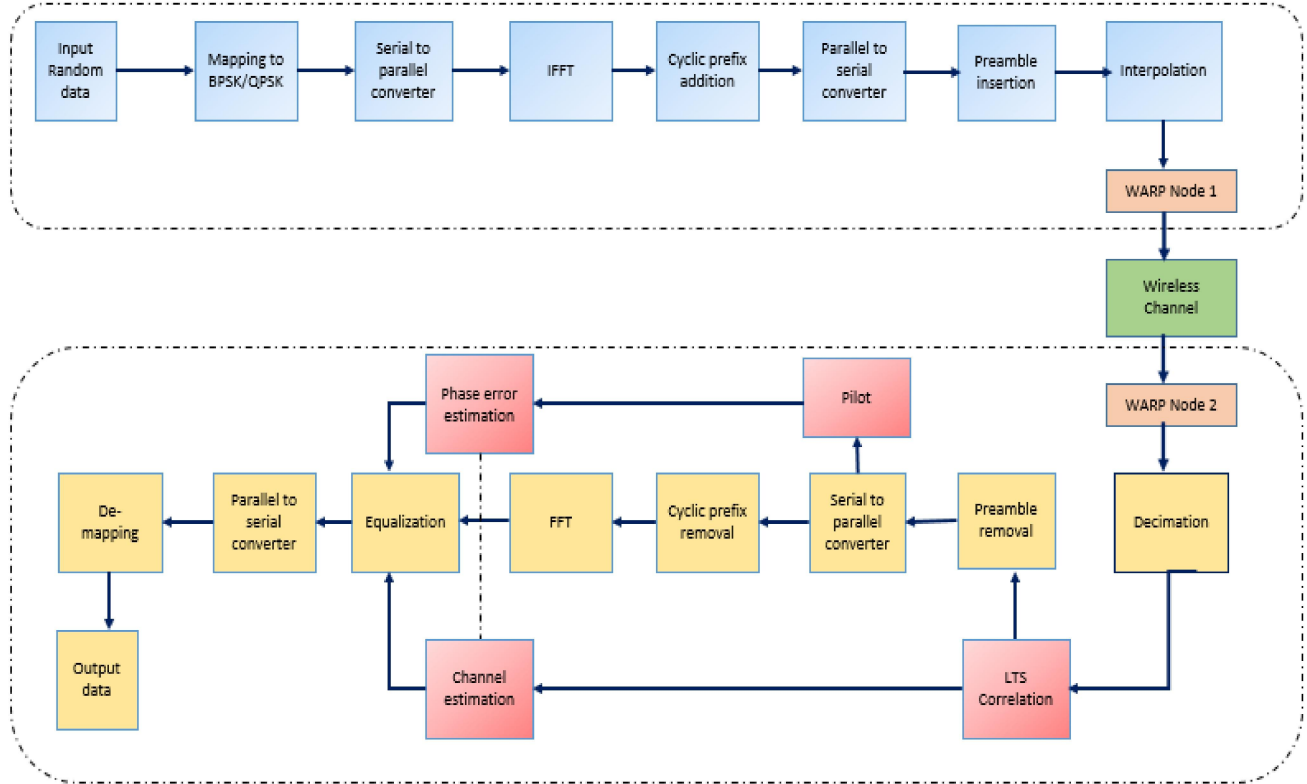
Fig.4.13. Block Diagram of OFDM System in WARP

Frame Design:

Frame design for communication using WARP is depended on several parameters [41]. For example, we have used the number of buffers in WARP as 2^{16} or 65536 samples, and the sampling rate of the system is considered as 40 MHz. This frame design process is to match the signal structure with the WARP specification. For each frame, some field should be imparted for delay margin. Mainly the origin of the delay is propagation delay and data acquisition in WARP, which is allocated as 896 samples. Delay will be located at the end of the frame in the form of zeros; hence this delay is called zero padding. The frame design for communication is shown in the figure below. Addition to this, all OFDM symbols not only contain some data but also cyclic-prefix, pilot or training symbol and virtual subcarrier.

A frame structure similar to the following in Fig.4.14 has been used in course of our experiments:
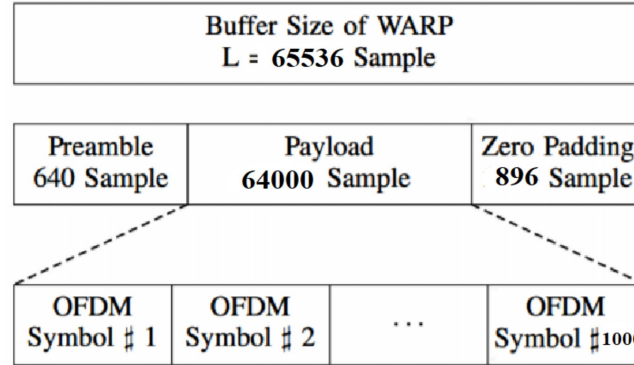
Fig.4.14. OFDM Frame Structure for Communication

Transmitter Side:

- The transmit data bit is mapped into values according to the type of modulation scheme, for BPSK the bit sequences consist of bits 1 and 0, which are mapped to the values ±1and for QPSK bit sequences are mapped to four complex values ±0.7071±i 0.7071, where $i = \sqrt{-1}$.

- Then, the sequence is divided into blocks consisting of N=1000, OFDM symbols per block, each block is converted into serial to parallel and each symbol will modulate sub-carriers. Here, we use 64 sub-carriers, with 48 sub-carriers allocated for data symbols, 4 for pilots and the rest are set to zeros.

- Next, the 64-point IFFT is performed to produce multi-carrier OFDM modulation, with adjacent sub-carrier spacing (1/T), where T is the OFDM symbol period.

- After the IFFT process, a cyclic prefix is added, where 25% of OFDM symbols are cyclically added for each symbol, i.e. the length is 16.

- The next process is addition of preamble. The preamble field consists of two parts [42], which are the Short Training Sequence (STS) and the Long

Training Sequence (LTS) with a total length of 16 μs. The 10 short training symbols are modulated with the elements of a known sequence using 12 subcarriers, while two long training symbols, consisting of 52 subcarriers, are also modulated with an a priori known sequence. The STS and LTS are used for packet detection and synchronization applications and to estimate the time and frequency offsets between a receiver and transmitter. This preamble is shown below.

| STS | STS | ... | STS | GI | LTS | LTS |

10 ×
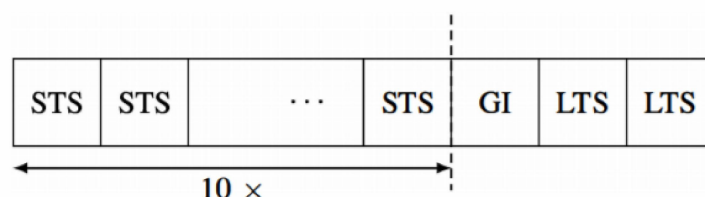
Fig.4.15. Preamble Structure

- LTS-based correlation methods can be used to obtain a fine estimate of the start sample of the LTS using the primary coarse estimate of the start sample of STS. Using the primary estimate of the start sample where the STS occurs (300 in this case) these correlation-based methods are applied to search the start sample of the LTS within the expected range of its occurrence. Herein, LTS-methods search from sample 400 (300+100) to detect the start sample. The LTS cross correlation method uses the normalized correlation between received samples and the known LTS (without the GI, i.e., Guard Interval). The CP-based method uses the correlation properties introduced by the 32 sample GI in the LTS to detect the start sample of the LTS (including the GI) whenever the normalized correlation value crosses a certain threshold.

- After that, the signal is interpolated to increase the sampling rate and then signal ready to be transmitted and is carried by higher frequency signal. The interpolation process is divided into two start up steps: up-sampling and low pass filtering (LPF).

- After this process, signal is normalized to improve Digital-to-Analog Converter (DAC) in WARP, such that the signal falls between range -1 to 1. Later, this signal is sent to the buffer transmitter through Ethernet. This transmission process will start after the synchronisation packet is sent to the transmitter node.

Receiver Side:

- In the receiver, the received signal will be decimated. The decimation process consists of two steps: low-pass filtering and down-sampling that is the opposite of up-sampling in the transmitter.

- After the decimation process, next step is cross correlation process between received preamble and LTS reference, the calculation of cross-correlation is using following equation:

- $C(n) = \sum_{l=0}^{M} \sum_{k=0}^{N} r(lN + k + n)s(lN + k)$ .... (4.1)

- Here, **r** is the total received preamble, **s** is one unit LTS, **N** is OFDM data length and **M** is number of cross correlated LTS. The cross-correlation process is performed for the synchronisation process so that the start of each frame can be determined. An example of the cross-correlation result is shown in the figure below. The two peak values in this figure indicate the LTS location.
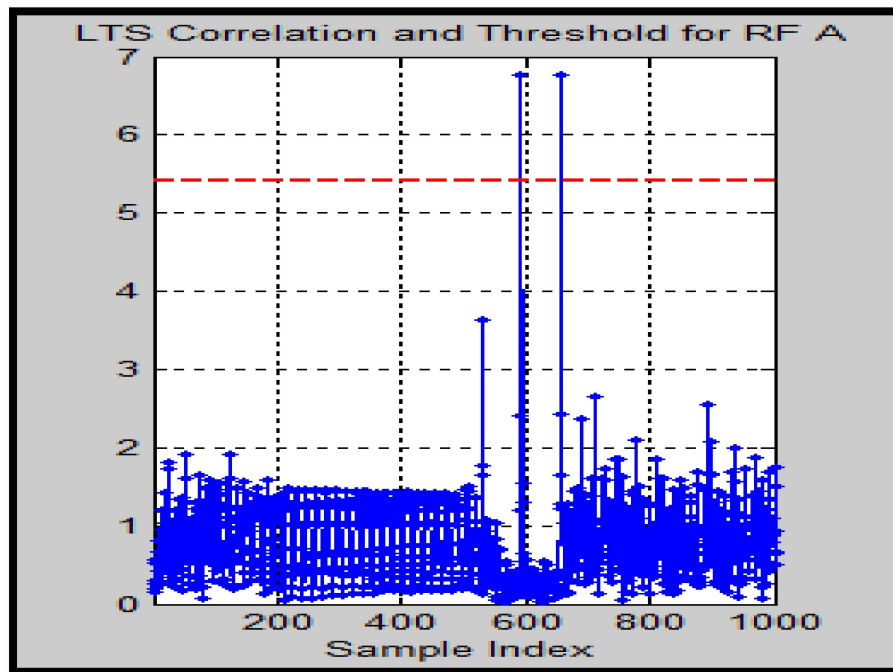
Fig.4.16: LTS Correlation

- After the beginning of the first OFDM frame in the receiver is known, the next step is removing the cyclic prefix part and then the FFT process is applied using 64-point FFT.

- Following FFT process is an equalizer process that is required to reverse the distortion incurred by a signal transmitted through a channel. With the cross-correlation and estimation results, the equalizer will equalize the magnitude and the phase response of the channel in frequency domain for reliable signal detection.

- Next, the de-mapping process is needed to get the bit estimation from the BPSK constellation.

Channel Estimation:

In the channel estimation process, the LTS after FFT processing is denoted as $R_{l,k}(l = 0, 1)$, and is expressed in the equation below, where the index $l = 0$ represents the first LTS, $l = 1$ for the second LTS and index k is the number of sub-carrier.

$$R_{1,k} = H_{1,k}d_{1,k} + W_{1,k} \qquad \ldots\ldots\ldots(4.2)$$

$W_{1,k}$ is noise signal after the FFT process, $d_{1,k}$ is transmitted LTS and $H_{1,k}$ is the channel frequency response. Then, the result of channel estimation using LTS can be found using following equation:

$$\hat{H}_k = \frac{1}{2}(R_{0,k} + R_{1,k})/d_k$$

$$= \frac{1}{2}(H_k d_k + W_{0,k} + H_k d_k + W_{1,k})/d_k$$

$$= \frac{1}{2}(W_{0,k} + W_{1,k})/d_k + H_k \qquad \ldots\ldots\ldots (4.3)$$

After finding the value of estimation channel, equalization process will be performed on the remaining received payload (total of all OFDM symbol) using equation:

$$x_e(k) = x(k)/\hat{H}_k \qquad \ldots\ldots\ldots (4.4) \text{ [Zero-forcing Equalization]}$$

Scatter plot in channel estimation process is shown in fig.4.17.

Phase Error Estimation:

Channel estimation process includes a phase error estimation process. This estimation is necessary to overcome a timing offset. With this error all symbols contained in OFDM symbols will fall in the incorrect location on the signal constellation. Phase error estimation process is quite straightforward, the received symbol is multiplied by $e^{-j\theta}$ as shown in the equation below, where θ is the phase estimation result.

$$s'(k) = s(k)e^{-j\theta} \qquad \ldots\ldots\ldots(4.5)$$

where s' (k) is a received signal after the phase correction process. The value of θ is obtained from the average of angle value differences between the received pilot signal with pilot reference.
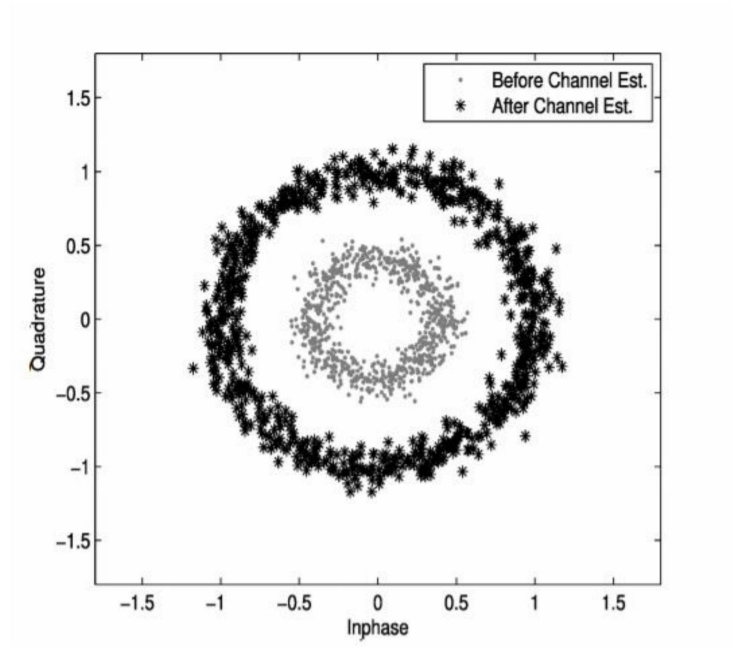
Fig.4.17. Scatter Plot in Channel Estimation Process

CFO, Phase Error and SFO:

Typically, a transmitter and receiver are each clocked independently. This independence manifests in three different degradations that must be dealt with by a wireless receiver:

- **Carrier Frequency Offset (CFO):**

  The centre frequency of the transmitter will not perfectly match the centre frequency of the receiver. Unless corrected, this will de-orthogonalize the OFDM subcarriers and cause inter-carrier interference (ICI). CFO is typically corrected in the time domain via multiplication with a digital carrier whose frequency negates the CFO estimate. This example uses a technique that compares two sequential preamble training symbols to estimate the CFO [43].

- **Phase Error:**

  Even after CFO is corrected in the time domain, there is typically a residual phase error component that must be corrected in the frequency domain and

tracked over time. OFDM systems employ multiple pilot subcarriers to enable this correction system. All data subcarriers in each OFDM symbol are phase-rotated to match any residual rotation observed in the known pilots.

- **Sampling Frequency Offset (SFO):**

The temporal duration of a sample is slightly different at the receiver and transmitter due to different sampling clocks. Over the course of a reception, the relative sample periods will drift apart from one another. This manifests as larger phase error for the outer subcarriers. Each data subcarrier in each OFDM symbol is phase-rotated differently according to its subcarrier index [44].

At the top of the script, there are three control variables that toggle three different correction systems:

- ➢ DO_APPLY_CFO_CORRECTION
- ➢ DO_APPLY_PHASE_ERR_CORRECTION
- ➢ DO_APPLY_SFO_CORRECTION

AGC (Automatic Gain Control) Target Gain:

The Tx path applies gain at three amplifiers [45]: Tx Base Band (Tx BB), Tx RF, and Tx RF PA (Power Amplifier). The Tx RF PA is always fixed at 30 dB gain. The Tx BB and Tx RF amplifiers are adjusted digitally, and the range of gains is the following:

1. Tx BB: In [0, 3] (coarse gain)

2. Tx RF: In [0, 63] (fine gain)

The Rx path applies gain at two amplifiers: Rx Base Band (Rx BB) and Rx RF. Rx amplifiers are adjusted digitally, the range of gains is the following:

1. Rx BB: In [0, 31] (fine gain)

2. Rx RF: In [0, 3] (coarse gain)

WARPLab includes the option to an automatic adjustment of receiver gains based on the power and structure of an incoming waveform [46].

➢ **Gain Selection based on RSSI and Received I/Q**

The **MAX2829** transceiver in WARP's radios has two stages of Rx gain:

A low noise amplifier (LNA) that can provide up to 30 dB of amplification followed by a baseband gain that can provide up to 63 dB of additional amplification. Together, these gain stages can provide up to 93 dB of gain to a received signal. The AGC core provided with WARPLAB selects these two gains in three sequential stages:

1. When triggered, the AGC first selects a Low Noise Amplifier (LNA) gain based on the Receive Signal Strength Indicator (RSSI) signal provided by the transceiver. It is done by first converting the digital RSSI measurement into an receive power estimate in dBm. With this value, the AGC goes for one of the three possible LNA gain settings that minimizes Error Vector Magnitude (EVM). The MAX2829 datasheet provides graphs that show EVM for each LNA gain setting as a function of receive power.

2. Changing the LNA gain affects the RSSI measurement. After RSSI has been settling from the previous LNA gain adjustment, the value is re-read and is used to make an initial, coarse, update to the baseband gain stage.

3. After both the LNA gain and the baseband gain have been adjusted based on RSSI, a final clarification of the baseband gain is made by the AGC based upon waveform's I and Q values themselves. Prior to this stage, the waveform cannot be trusted for an accurate power measurement since it is likely saturating the radio's ADCs. Using the waveform's I and Q values to refine the baseband gain introduces an important waveform dependence. During the window that the AGC inspects the I/Q waveform,

the magnitude of the signal must be periodic in 16 40-MHz samples. A series of 20 MHz-wide 802.11 STS symbols meets these requirements.

➢ **AGC Function description:**

agc_target : This command in WARPLAB adjusts the target gain of the AGC. A lower (i.e. "more negative") value will produce a smaller signal at the ADCs and vice versa.

Set the AGC target

Arguments: (int32 target) target: target receive power (in dBm) default value: -16

Returns: none

This command is the best way to adjust AGC behaviour to apply more or less gain. For example, a target of -8dBm will apply more gain than a target of -11dBm, so the waveform will be larger at the inputs of the I and Q ADCs.

4.6 Comparative Analysis of power measured at RF Port A of WARP Board under 2.4GHz and 5 GHz frequency bands

Frequency bands are referred to as radio waves that transfer data wirelessly between devices. The 802.11 standard provides several distinct radio frequency bands among which WARP testbed makes use of 2.4 GHz /5GHz ISM/UNII bands for wideband wireless communication. The frequency band/channel and corresponding centre frequency map is mentioned below in table 4.2 [47]:

Table 4.2: Band/Channel - Centre Frequency Map:

2.4 GHz		5 GHz	
Channel	**Frequency**	**Channel**	**Frequency**
1	2.412	1	5.180
2	2.417	2	5.190
3	2.422	3	5.200
4	2.427	4	5.220
5	2.432	5	5.230
6	2.437	6	5.240
7	2.442	7	5.260
8	2.447	8	5.270
9	2.452	9	5.280
10	2.457	10	5.300
11	2.462	11	5.310
12	2.467	12	5.320
13	2.472	13	5.500
14	2.484	14	5.510
		15	5.520
		16	5.540
		17	5.550
		18	5.560
		19	5.580
		20	5.590
		21	5.600
		22	5.620
		23	5.630
		24	5.640
		25	5.660
		26	5.670
		27	5.680
		28	5.700
		29	5.710
		30	5.720
		31	5.745
		32	5.755
		33	5.765
		34	5.785
		35	5.795
		36	5.805
		37	5.825
		38	5.560
		39	5.870
		40	5.875
		41	5.880
		42	5.885
		43	5.890
		44	5.865

While comparing the 2.4GHz and 5GHz frequency bands the first one covers a larger area and provides a more extended range than the 5GHz band, but with lower data rates. On the other hand, the 5GHz band provides a smaller coverage area than the 2.4 GHz band but with a higher data rate. Thus, when the frequency increases, its ability to penetrate solid objects (like walls) decreases and due to this reason the 5GHz band was used mostly in outdoor deployments at the beginning.

Interference is one of the potential attributes in wireless communication which can slow down a network significantly and reduce its scope as well. For the 2.4GHz band, the two most obvious sources of wireless network interference are wireless telephones and microwave ovens. Whereas, for the 5GHz band, cordless phones, radars, digital satellite and perimeter sensors are the most generic sources of interference.

When multiple devices utilize the same frequency, the effect of interference becomes a cardinal concern in case of receiver signal characteristics and it eventually reduces the connection speed. The waves used by the 2.4GHz band are suitable for long distance communication through walls and solid objects. Therefore, 2.4GHz is more convenient if one needs to provide a better scope on the devices or have many walls or other objects where one needs coverage.

On the other side, the short waves of 5GHz band make it less capable of going through walls and solid objects. This happens because of the characteristics of electromagnetic wave i.e., at higher frequencies (5GHz), waves attenuate strongly. Hence, the signal is easily influenced by different obstacles like walls, floor, ceiling, doors, and others. In this context we have performed the analysis of system BER considering both 2.4 GHz and 5GHz frequency range. The measurement of RF port A power of WARP transmitter board is enlisted below in table 4.3.

Table 4.3: RF Port A transmit power measurement for 2.4GHz and 5GHz frequency range

RF GAIN	POWER (dBm) at RF A (Cable loss= 2dBm) Centre frequency = 2.412 GHz	POWER (dBm) at RF A (Cable loss = 2dBm) Centre frequency = 5.18 GHz	RF GAIN	POWER (dBm) at RF A (Cable loss= 2dBm) Centre frequency = 2.412 GHz	POWER (dBm) at RF A (Cable loss =2dBm) Centre frequency = 5.18 GHz
0	-31.89	-34.7	33	-15.45	-19.99
1	-32.08	-34.65	34	-14.54	-19.16
2	-31.72	-34.85	35	-14.59	-19.02
3	-31.76	-34.75	36	-13.45	-17.88
4	-31.05	-33.71	37	-13.33	-18.03
5	-31.2	-33.61	38	-12.23	-16.71
6	-30.07	-32.7	39	-12.21	-16.75
7	-29.6	-32.7	40	-11.29	-15.63
8	-29.08	-31.98	41	-11.46	-15.58
9	-28.63	-31.96	42	-10.44	-14.51
10	-27.54	-31.02	43	-10.31	-14.46
11	-27.85	-31.16	44	-9.23	-13.34
12	-26.8	-30.29	45	-9.16	-13.32
13	-25.38	-30.08	46	-8.18	-12.19
14	-24.72	-29.25	47	-8.22	-12.17
15	-24.62	-29.21	48	-7.63	-11.51
16	-24.03	-28.19	49	-7.2	-10.94
17	-23.98	-28.25	50	-6.69	-10.37
18	-22.91	-27.35	51	-6.14	-9.94
19	-22.79	-27.34	52	-5.72	-9.31
20	-21.72	-26.15	53	-5.08	-8.75
21	-21.71	-26.15	54	-4.53	-8.22
22	-20.85	-25.25	55	-4.12	-7.7
23	-20.76	-25.39	56	-3.74	-7.12
24	-19.84	-24.33	57	-2.99	-6.68
25	-19.72	-24.15	58	-2.52	-6.2
26	-18.81	-23.15	59	-2.04	-5.84
27	-18.86	-23.15	60	-1.41	-5.46
28	-17.78	-21.91	61	-1	-5.27
29	-17.77	-21.94	62	-0.54	-4.55
30	-16.83	-20.97	63	0.02	-4.12
31	-16.84	-20.99			
32	-15.53	-20.15			

It is clearly visible from the above table that transmitted power at Port A in case of 2.4GHz is larger than that of 5GHz range for each value of RF gain. It can be extrapolated that attenuation is higher in case of high frequency band.

Table 4.4: Parameters used for two-user PD NOMA model implementation in WARP Board

Parameters	Values
Distance of near user (UE1)	0.86 m
Distance of far user (UE2)	2.7 m
Power allocation factor of UE1	0.15 (BPSK) ,0.27 (QPSK),0.4(Adaptive)
Power allocation factor of UE2	0.75 (BPSK) ,0.73 (QPSK),0.6(Adaptive)
Transmit power at RF port A of WARP Board	-18.78 dBm
AGC target gain	-8 and -11
Channel ID	1
Frequency range	Centre frequency: 2.412 GHz Start Frequency: 2.401 GHz Stop Frequency: 2.423 GHz
No. of OFDM symbols	1000
No. of subcarrier in OFDM	64
Cyclic prefix length	16

Table 4.5: Parameters used for three-user PD NOMA model implementation in WARP Board

Parameters	Values
Distance of near user (UE1)	0.85 m
Distance of middle user (UE2)	1.5 m
Distance of far user (UE3)	2 m
Power allocation factor of UE1	0.02 (BPSK, QPSK, Adaptive-two BPSK, Adaptive-two QPSK)
Power allocation factor of UE2	0.18 (BPSK, QPSK, Adaptive-two BPSK, Adaptive-two QPSK)
Power allocation factor of UE3	0.80 (BPSK, QPSK, Adaptive-two BPSK, Adaptive-two QPSK)
Transmit power at RF port A of WARP Board	-18.78 dBm
AGC target gain	-13 and -19
Channel ID	1
Frequency range	Centre frequency: 2.412 GHz Start Frequency: 2.401 GHz Stop Frequency: 2.423 GHz
No. of OFDM symbols	1000
No. of subcarrier in OFDM	64
Cyclic prefix length	16

4.7 Result Analysis

4.7.1   Power allocation strategy

Fig.4.18 and Fig.4.19 represent the distribution of BER for both near user and far user with respect to power allocation coefficient of near user under different modulation techniques. Fig.4.19 helps to find out range of power allocation for both the users which provides the least system BER. With this inference we have chosen different values of power coefficient for different modulation techniques for 2.4 GHz frequency range which are enlisted in parameter table 4.1. We have observed that for only BPSK modulation scheme power allocation coefficient for near user 1 (α_1) is 0.15 whereas value of α_1 in case of QPSK modulation scheme is 0.27. This can be explained as for QPSK bit error rate is higher than that of BPSK, hence if the near user is allocated with more power in case of QPSK then the BER will be as less as possible.
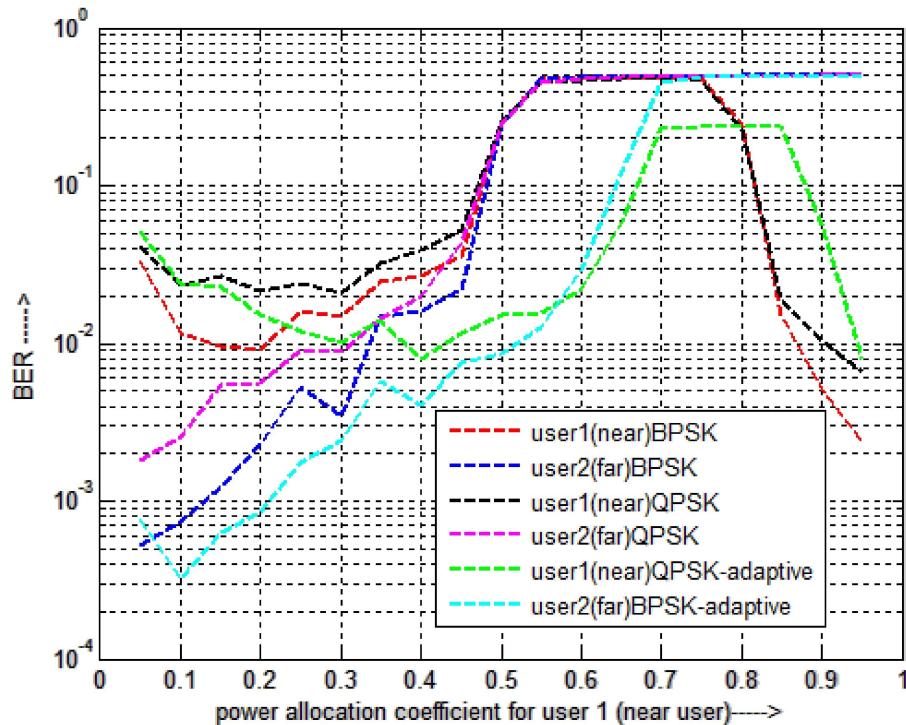

Fig.4.18. Bit error rate with respect to power allocation coefficient for user1 in two-user downlink PD-NOMA model
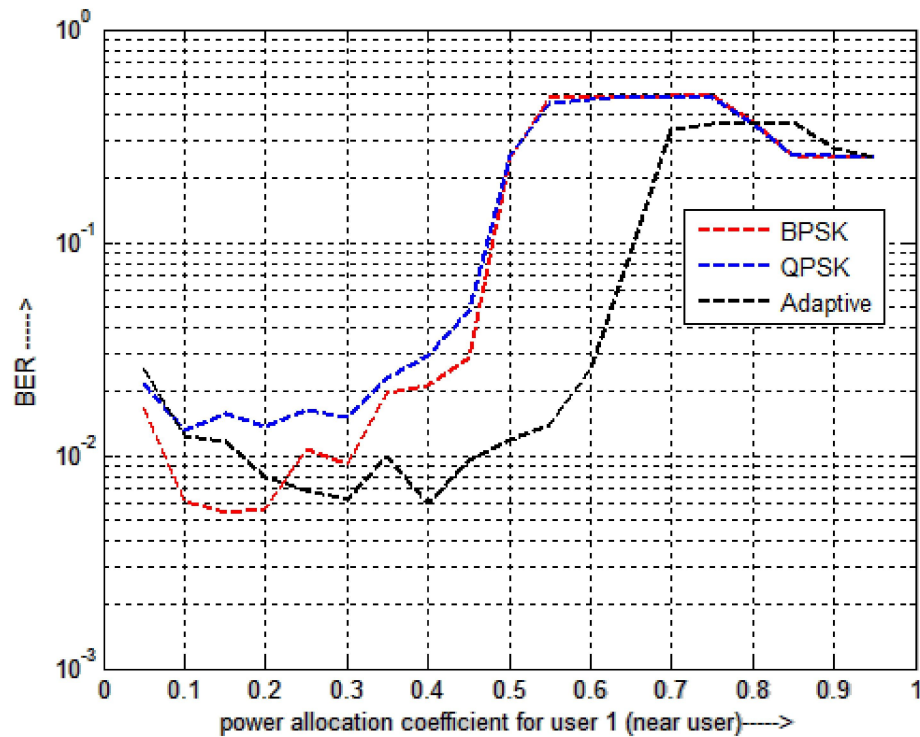
Fig.4.19. Bit error rate with respect to power allocation coefficient for user 1 in two-user downlink PD-NOMA model under different modulation technique

4.7.2   Constellation diagram

- *Constellation diagram for two-user PD NOMA model for 2.4GHz band under target AGC gain -13dBm*
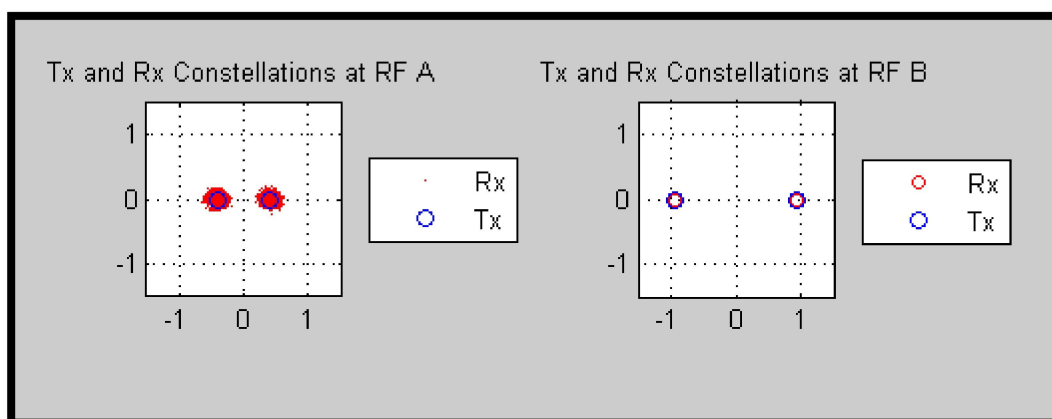

Fig.4.20. Constellation diagram of two users under only BPSK modulation scheme

Fig.4.21. Constellation diagram of two users under only QPSK modulation scheme

Fig.4.22. Constellation diagram of two users under only ADAPTIVE modulation scheme

- *Constellation diagram for two-user PD NOMA model for 5GHz band under target AGC gain -13dBm*

Fig.4.23. Constellation diagram of two users under only BPSK modulation scheme
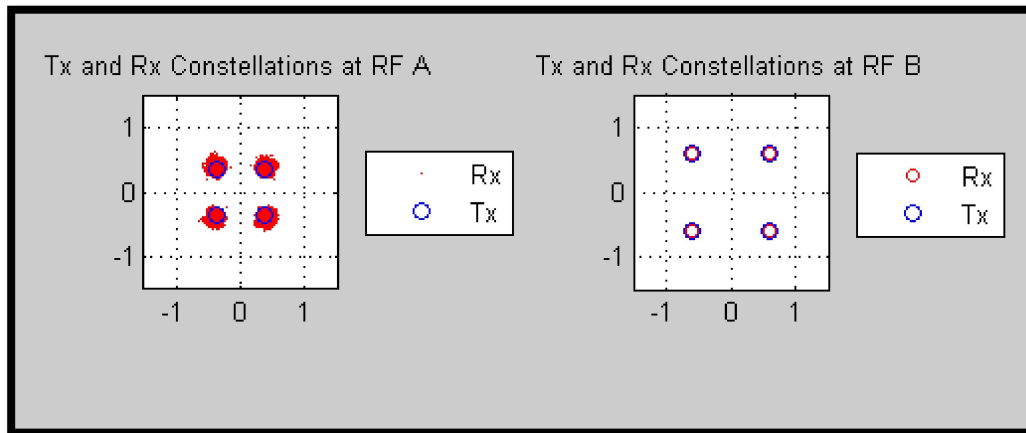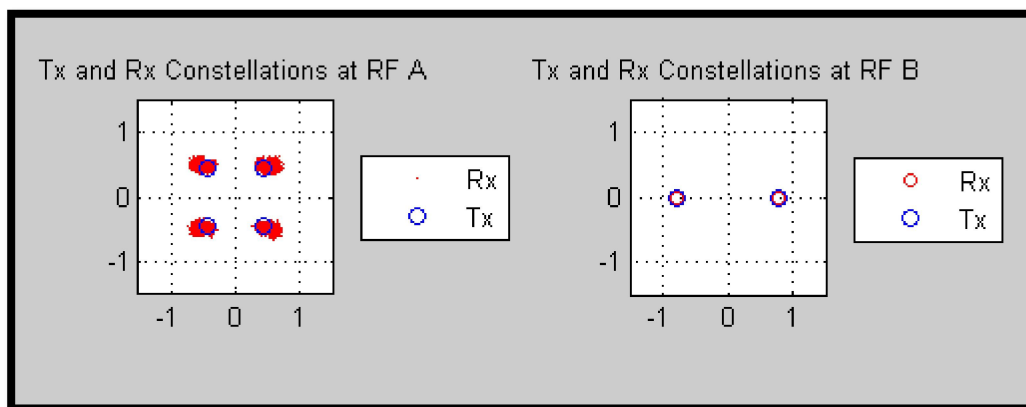

Fig.4.24. Constellation diagram of two users under only QPSK modulation scheme

Fig.4.25. Constellation diagram of two users under only ADAPTIVE modulation scheme

• *Constellation diagram for three-user PD NOMA model for 2.4GHz band under target AGC gain -13 dBm*
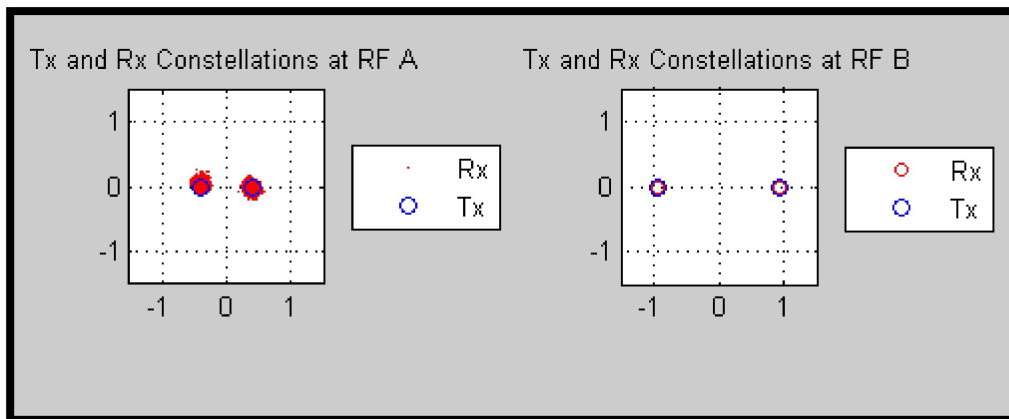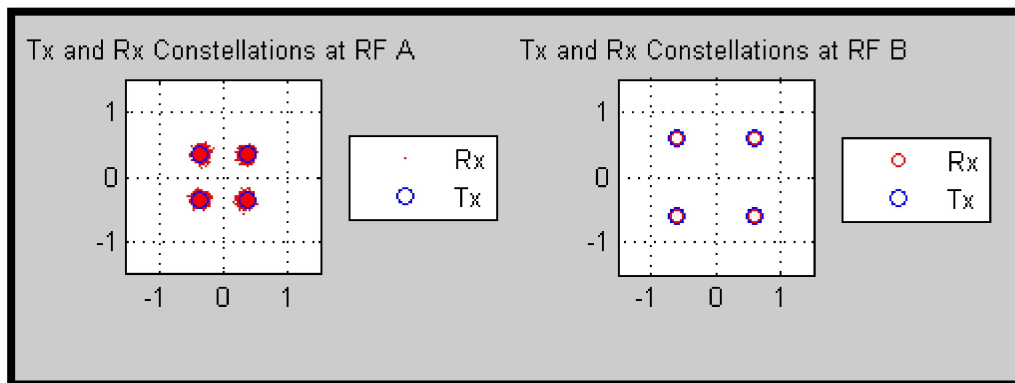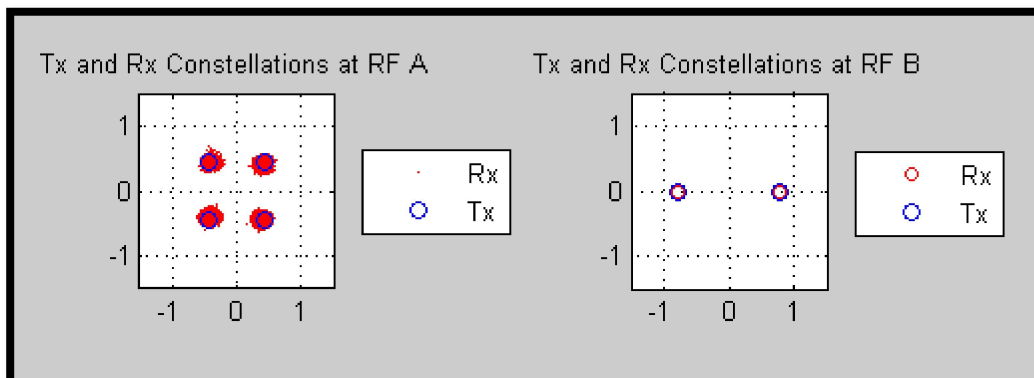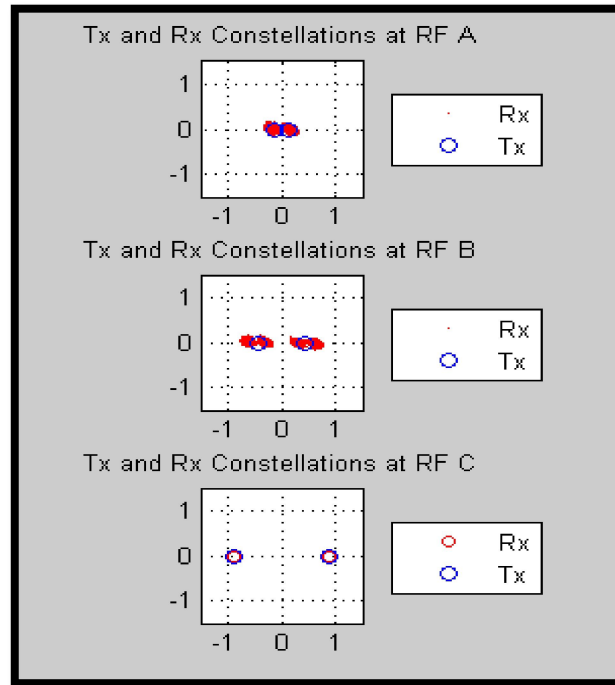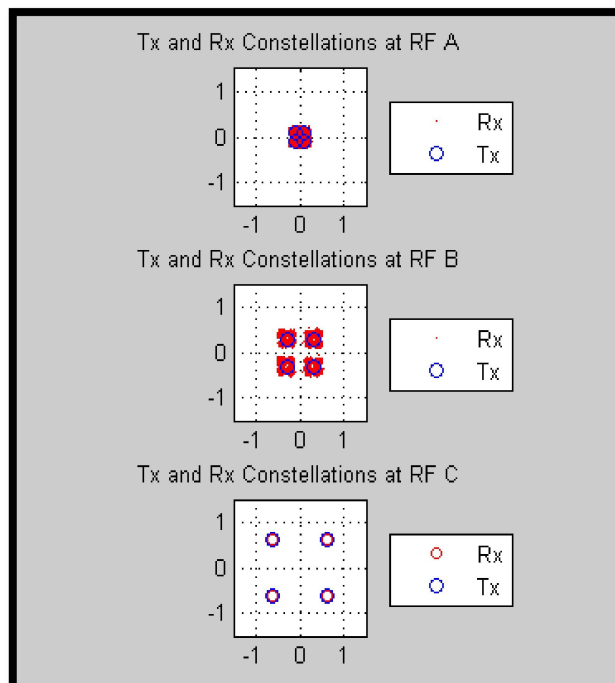

a.

b.

Fig.4.26. Constellation diagram of three users under a. only BPSK modulation scheme b. only QPSK modulation

a.   b.
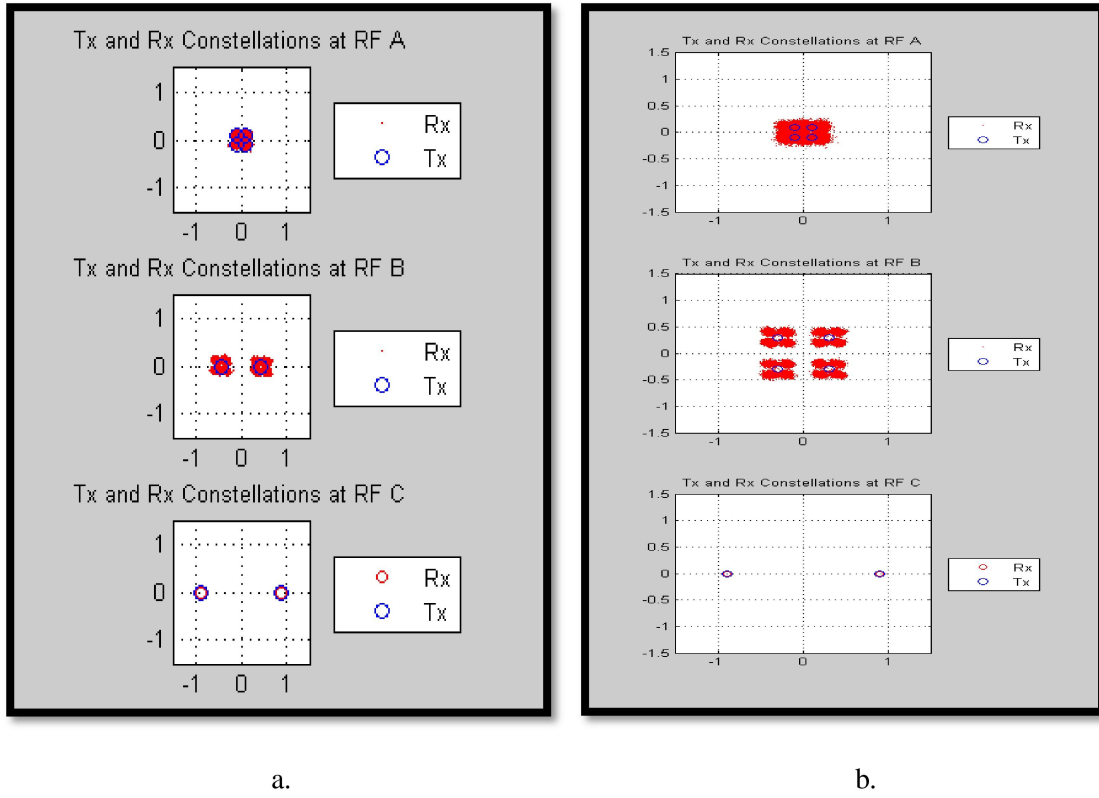
Fig.4.27. Constellation diagram of three users under a. Adaptive (two BPSK) modulation scheme   b. Adaptive (two QPSK) modulation

4.7.3   BER performance analysis of two-user downlink PD-NOMA model in 2.4 GHz and 5GHz frequency band

The values of α_1 considered for BPSK, QPSK and Adaptive modulation techniques are 0.15, 0.27 and 0.4 respectively. The analysis of system BER is performed within the limited range of transmit power (-33dBm to -19dBm) measured at RF port of WARP transmitter board. All the measurements have been carried out on Channel ID 1 having center frequency 2.412 GHz in the 2.4 GHz range. The measurements of BER under 5GHz frequency band are also performed on Channel ID 1 having center frequency 5.18 GHz within the limited transmitted power range (-34dBm to -23 dBm).

The results of test-bed measurements regarding the BER performance with respect to transmit RF power of WARP board are shown in Fig.4.28 to Fig.4.36.

Fig.4.28. BER vs. Transmit power for two user PD NOMA for AGC target gain -8 dBm in 2.4GHz range

Fig.4.29. BER vs. Transmit power for two user PD NOMA for AGC target gain -8 dBm in 2.4GHz range

Fig.4.30. BER vs. Transmit power for two user PD NOMA for AGC target gain -8 dBm in 2.4GHz range
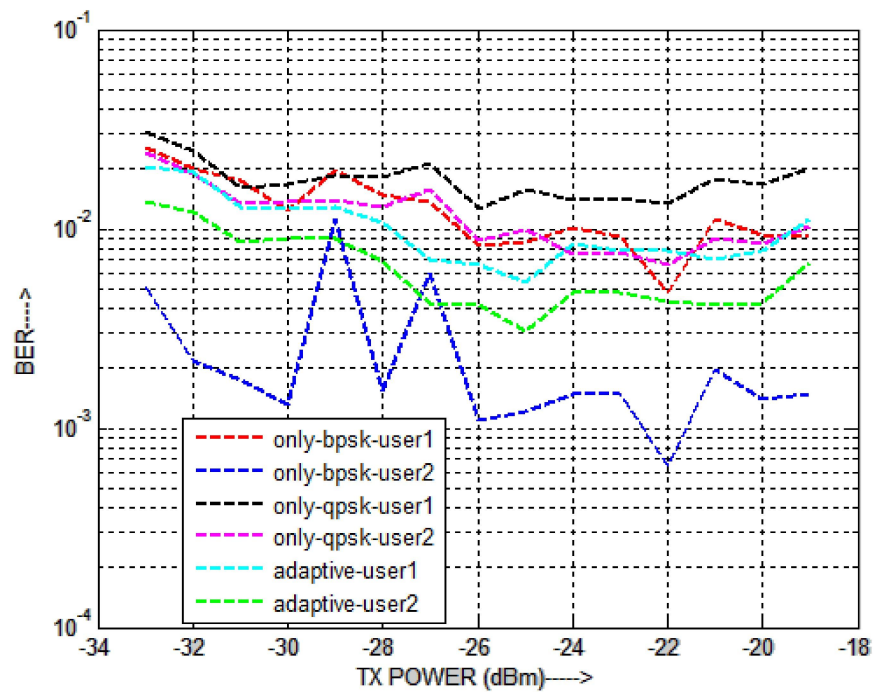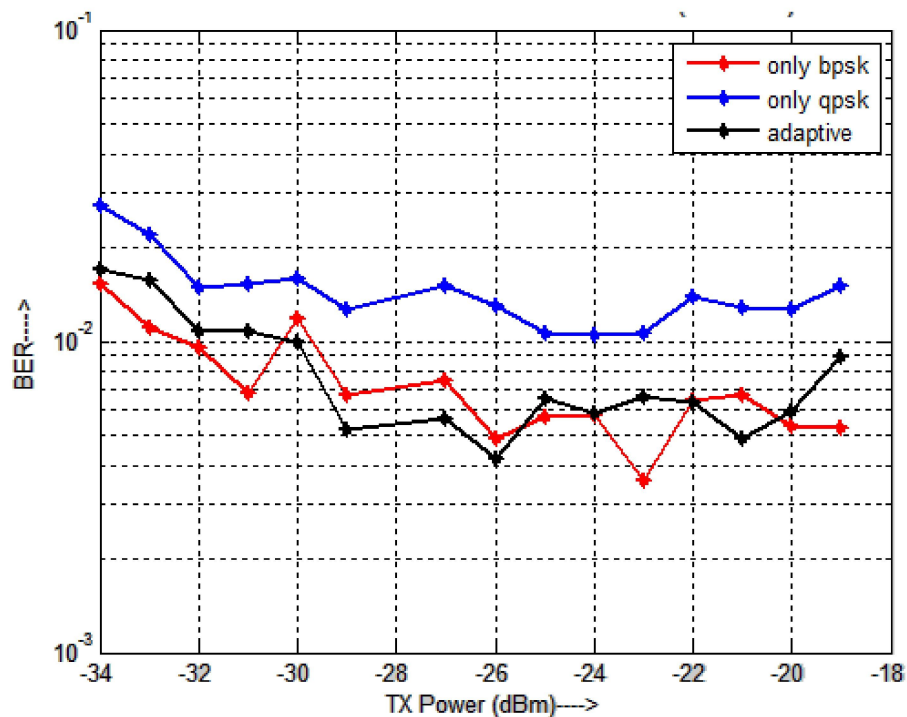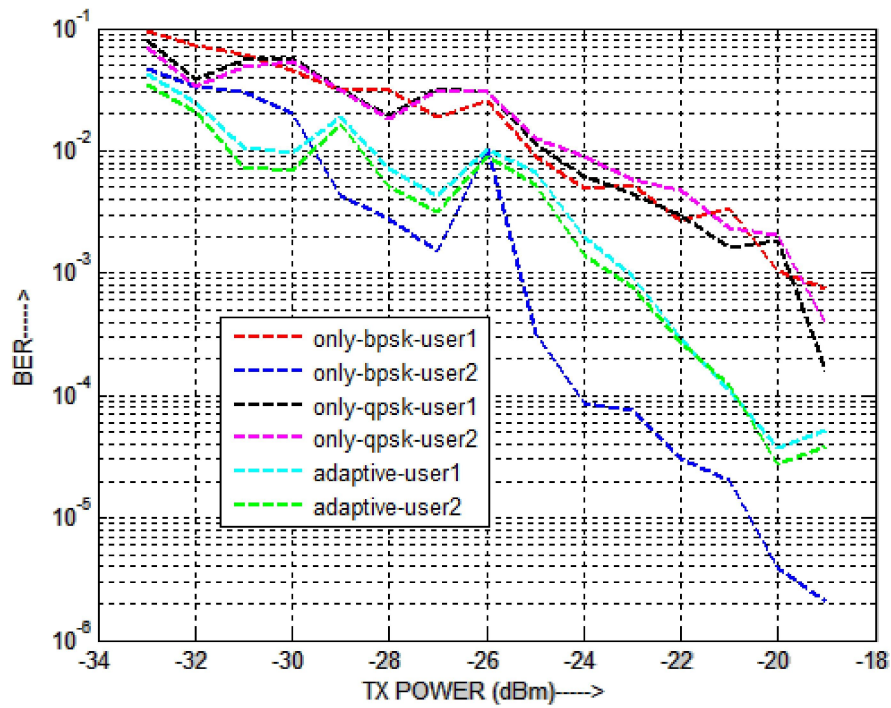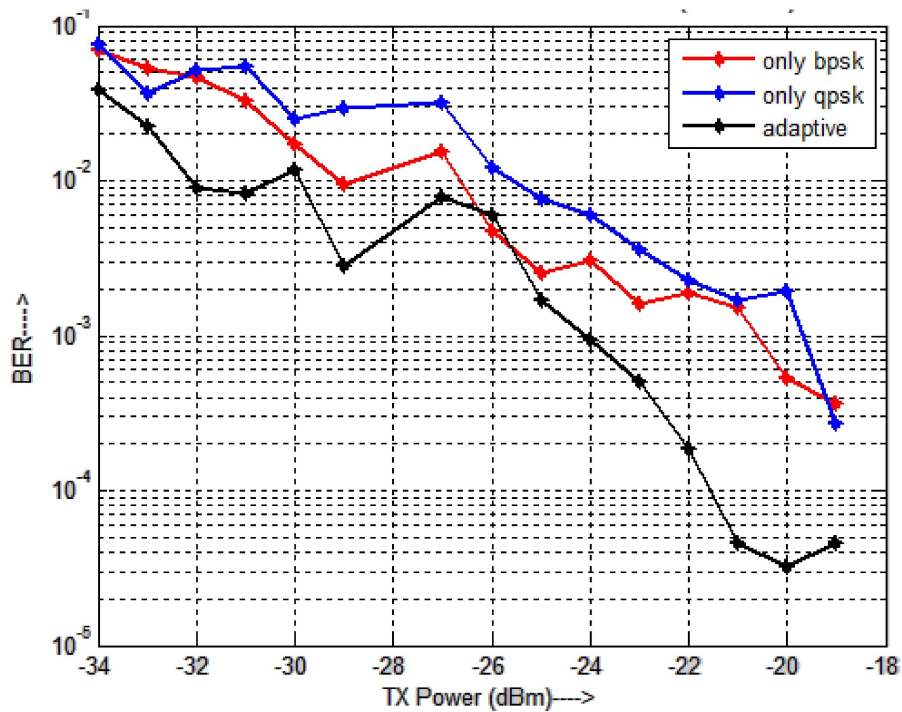

Fig.4.31. BER vs. Transmit power for two user PD NOMA for AGC target gain -8 dBm in 2.4GHz range
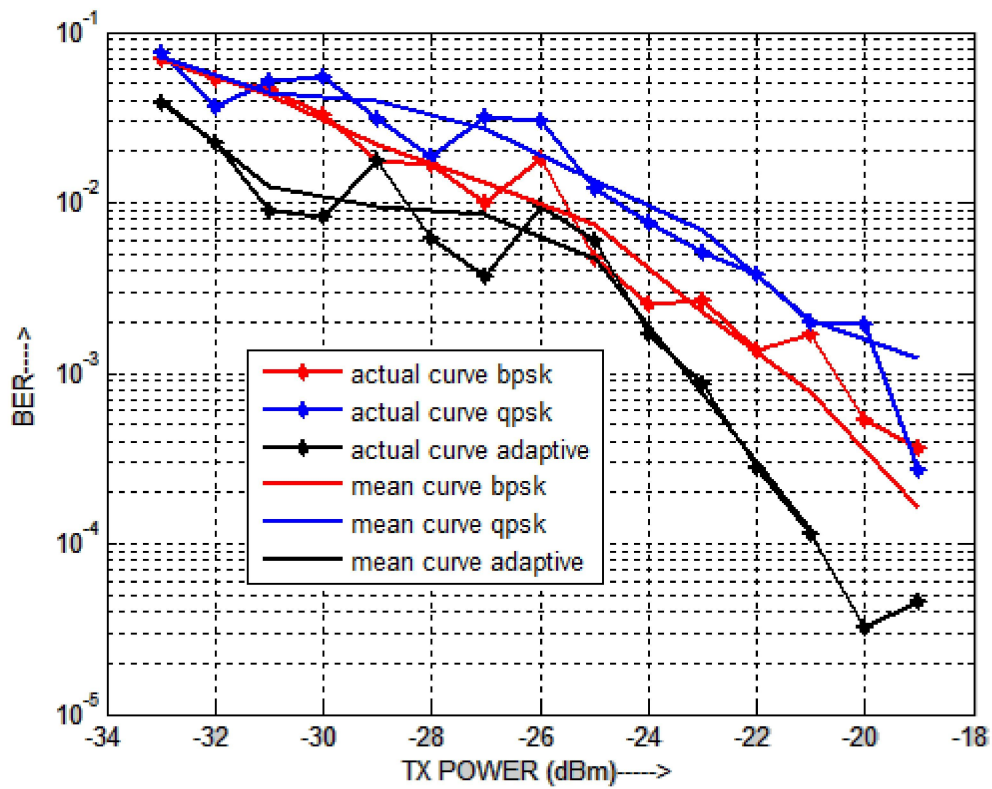
Fig.4.32. BER vs. Transmit power for two user PD NOMA with mean curve in 2.4GHz range
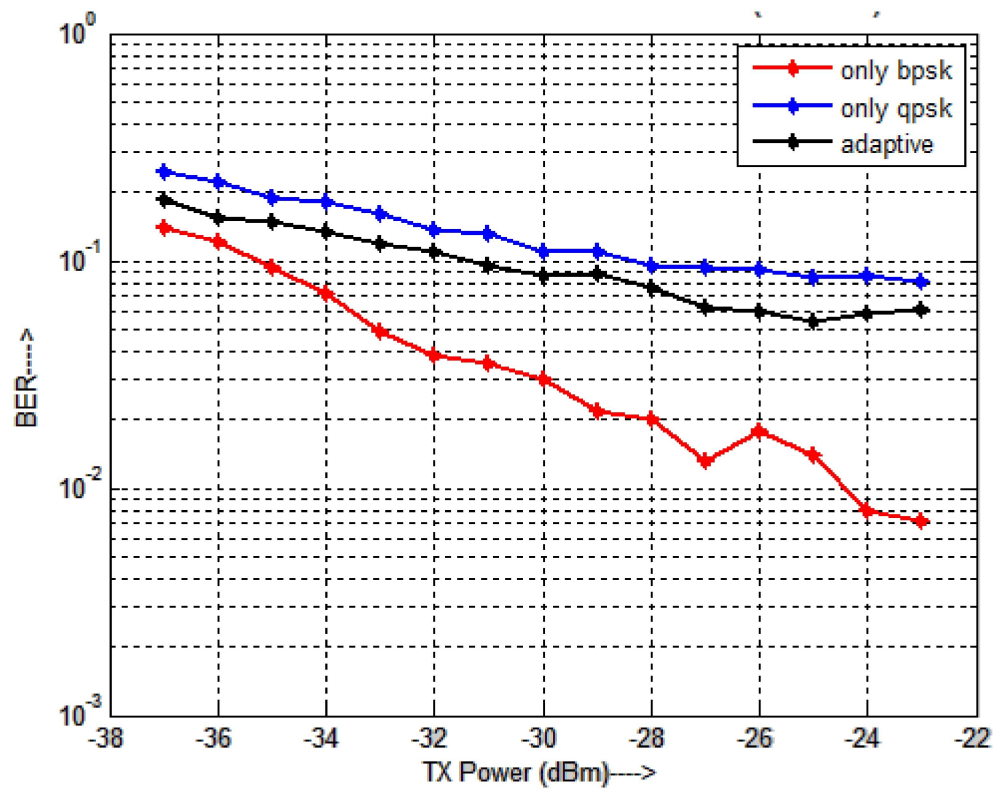
Fig.4.33. BER comparison plot for AGC Target gain -8 dBm (2 Users) in 5GHz range
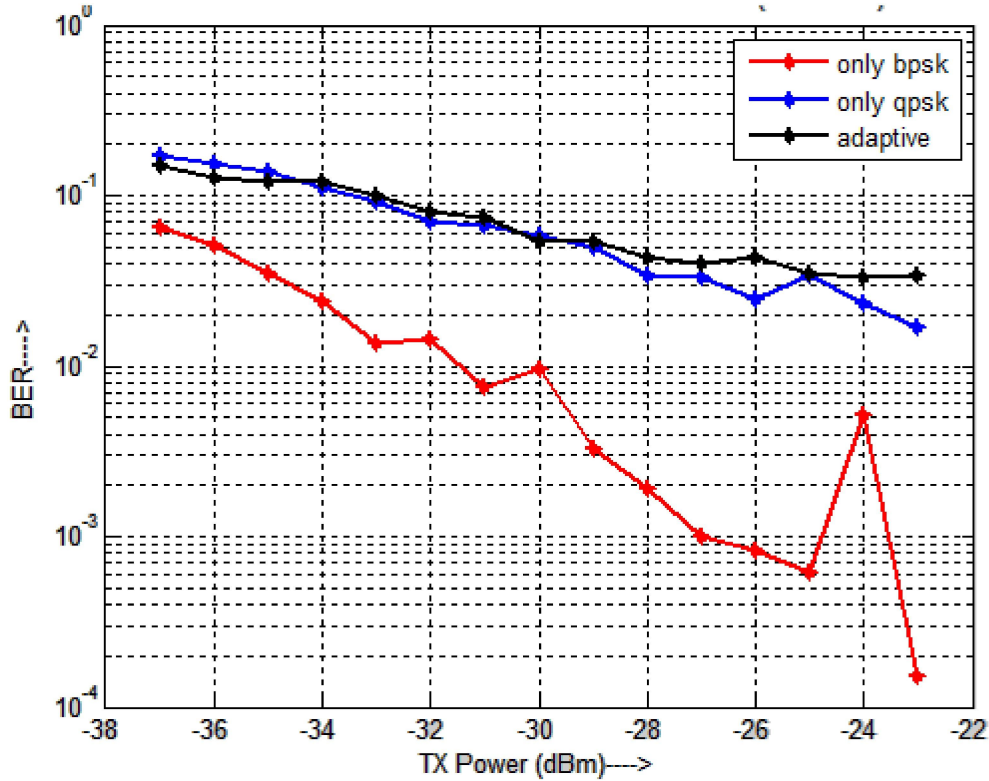
Fig.4.34. BER comparison plot for AGC Target gain -11 dBm (2 Users) in 5GHz range

Comparison of BER plots for different modulation schemes are presented in Fig.4.29 where it is observed that due to high target AGC gain i.e. -8 bit error rate curve can hardly follow the traditional falling with respect to transmit power. Hence the BER performance under different modulation techniques is incomprehensible where both the graphs for BPSK and ADAPTIVE approach are intended to over cross each other. The nature of the zigzag curve is ascribed to the indoor fading environment. Hence, the BER performance is also carried out considering AGC target gain -11 which is given in Fig.4.31. This plot clearly exhibits the traditional water falling curve of BER with respect to transmit power.

It also showcases that the system BER for adaptive modulation technique is the lowest thereby indicating that this modulation scheme is indeed useful for PD-NOMA in terms of BER considering the AGC target gain -11. Fig. 4.32 also

shows the variation of BER curve with respect to the mean BER curve for respective modulation schemes. It is due to the indoor fading environment that leads to multipath propagation and hence, the BER varies with respect to the local mean, at any point of time. The smoothness of the curve can be achieved with perfect channel estimation techniques. In our case considering more no. of BER readings (180) in order to get the average BER curve we have obtained almost smooth curve for BER under 5 GHz frequency shown in Fig.4.33 and Fig.4.34 with still having some glitches.

The comparison graph of BER under 5 GHz frequency band is observed in Fig 4.33 and 4.34. It has been noticed in Fig 4.33 and 4.34 that both the BER curves under only BPSK modulation scheme are exhibiting sharp fall up to the value of 10^{-3} and 10^{-4} considering the agc target gain as -8dB and -11dB respectively which shows that due to increase in agc target gain bit error rate decreases significantly As interference effect is severe for higher frequency, modulation technique (BPSK) which exhibits low BER becomes dominant. The graph for Only QPSK modulation scheme provides the highest BER value as expected. So, it is very crucial to select a higher order modulation technique which severely affects the system BER. Hence, we have incorporated the BER performance analysis under ADAPTIVE modulation approach for PD-NOMA which can be beneficial rather than using ONLY higher order modulation scheme for the users participating in NOMA.

4.7.4　　BER performance analysis of three-user downlink PD-NOMA model in 2.4 GHz frequency band

Performance analysis of system BER for three-user downlink PD-NOMA is carried out considering a fixed power allocation technique in 2.4 GHz band. The parameters used for the signal processing in MATLAB is enlisted in table 4.5.

The lowest system BER value under only BPSK modulation technique is very high for three-user NOMA system as compared to two-user model. As the number of users participating in PD-NOMA increases the power allocation to each user should be optimized in order to have less system BER. The glitches of those curves indicates the presence of multipath fading effect. Fig.4.35 and Fig.4.36 shows that adaptive modulation approach such as **TWO BPSK** and **TWO QPSK** scheme provides better BER performance rather than **ONLY QPSK** modulation scheme.
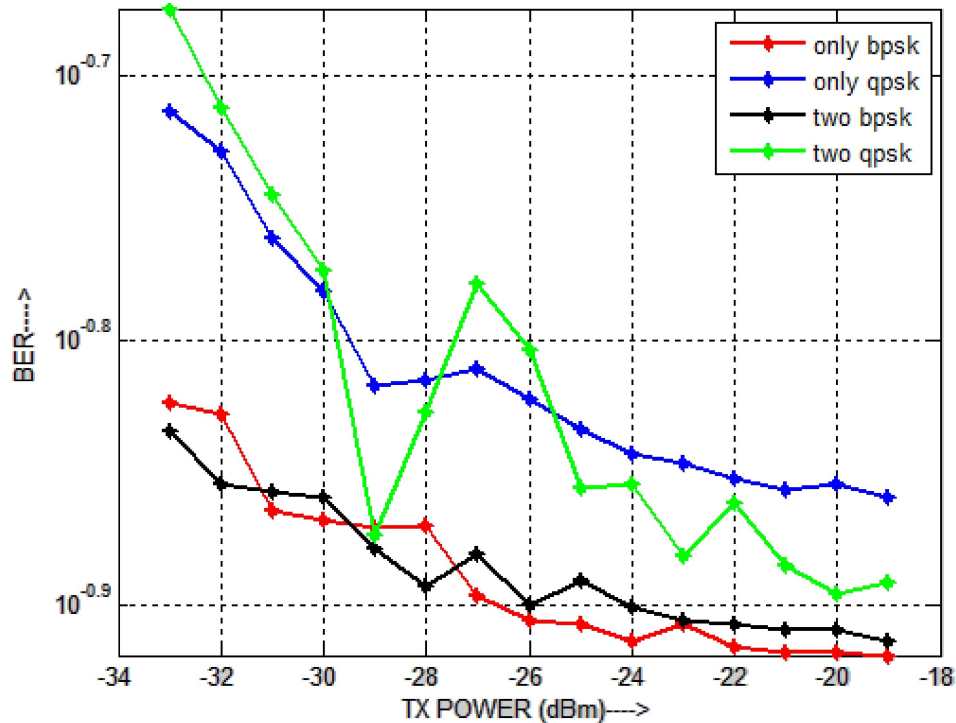

Fig.4.35. BER comparison plot for AGC Target gain -13 dBm (3 Users) in 2.4GHz range
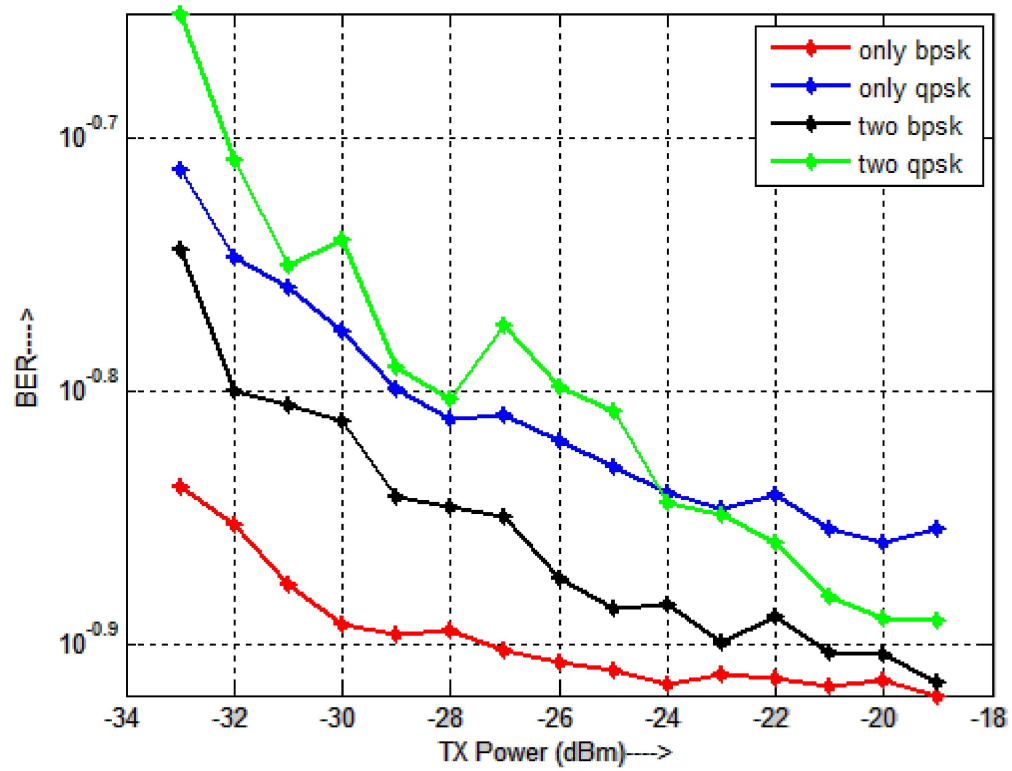
Fig.4.36. BER comparison plot for AGC Target gain -19 dBm (3 Users) in 2.4GHz range

Table 4.6 Result analysis of two-user PD-NOMA model

Frequency Range	AGC target gain	Suitable modulation Techniques	Remark
2.4 GHz	-8	BPSK and ADAPTIVE scheme	• BER curve hardly follows traditional water falling curve. • Analysis is incomprehensible as both the graphs for BPSK and ADAPTIVE approach are intended to over cross each other
	-11	ADAPTIVE scheme (near user: QPSK far user: BPSK)	• System BER for adaptive modulation is the lowest (approximately 10^{-4})
5 GHz	-8	Only BPSK	• System BER for ONLY BPSK modulation is the lowest (approximately 10^{-2}) • As interference effect is severe for higher frequency BPSK which provides lowest BER becomes dominant.
	-11	Only BPSK	• System BER for ONLY BPSK modulation is the lowest (approximately 10^{-3})

Table 4.7 Result analysis of three-user PD-NOMA model

Frequency Range	AGC target gain	Suitable modulation Techniques	Remark
2.4 GHz	-8	ONLY BPSK and ADAPTIVE (TWO BPSK: near user: QPSK and middle and far user: BPSK) scheme	• System BER for adaptive modulation and only BPSK provide lower values (approximately both $10^{-0.9}$ and $10^{-0.9}$). • The lowest system BER value under only BPSK modulation technique is very high for three-user NOMA system as compared to two-user model. As the number of users participating in PD-NOMA increases the power allocation to each user should be optimized in order to have less system BER.
	-11	ONLY BPSK and ADAPTIVE (TWO BPSK: near user: QPSK and middle and far user: BPSK) scheme	

Analyzing table 4.7, it has been observed that the system BER for three-user PD-NOMA model is hardly acceptable as it possesses very high value approximately in $10^{-0.9}$ range. This is due to the fact that we have considered fixed power allocation technique to the users. While increasing the number of users the power allocation should be optimized in such a way that system BER should not be affected severely. The convex optimization algorithm can be developed for strategic power allocation. Due to short time span we are hardly able to convey an optimization technique to improve the system BER performance in this thesis but we are considering in this our ongoing research on NOMA.

4.8 Chapter Summery

- For all the case the Bit Error Rate decreases with increasing transmitted power. However, the plot obtained does not give a smooth waterfall curve according to the theoretical convention. This can be improved upon by collecting a larger number of data points for averaging in future.

- For two-user model with the target AGC gain -11 dBm in 2.4GHz range, system BER possesses the least value in case of ADAPTIVE modulation approach where the near user is employed with higher order modulation technique, i.e., QPSK and BPSK, a lower order modulation scheme, is provided to the far user.

- The experimental validation of the fact that power loss is more while considering 5GHz frequency band is depicted in this chapter. Due to this reason system BER approaches the least value for ONLY-BPSK modulation scheme rather than ADAPTIVE approach under the consideration of both the AGC target gain -8 dBm and -11 dBm.

- For three-user model the BER graphs exhibit better performance of system BER in case of ADPATIVE approach rather than ONLY-QPSK scheme.

- It is a noteworthy discussion that the BER curve shows better performance in case of lower AGC target gain. Due to increase in AGC gain, received power also gets increased. If the target received power becomes very high then there will also be high increase in both the signal power as well as noise power with the help of LNA at receiver front end. Though LNA itself is used to minimize additional noise, the significant increment of AGC target gain leads to high distortion at received signal which can put a thrust to system bit error rate.

Chapter 5   Conclusion and Future Work

5.1 Conclusion:

In this thesis, we have studied the power domain NOMA system for downlink channel both in simulation and through a real time testbed implementation using WARP transceiver system, a software defined radio kit. At first, we have analyzed the PD-NOMA in its mathematical form and then performed simulation study in detail with respect to different modulation schemes.

The BER performance analysis under MATLAB simulation has taken care of one of the most severe issues in PD-NOMA i.e., power allocation technique. The simulation results are produced using both fixed and optimization power allocation technique. Another important notion of simulation in this thesis is to study an important observation that if higher order modulation schemes are applied to users, far from the base station, then there is a high chance of increase in BER for those users' data. Hence, higher order modulation schemes are preferable to apply on users nearer to the base station. This observation leads us to study a new modulation scheme i.e., an ADAPTIVE modulation technique, where near user is provided with higher order modulation technique such as QPSK and far user is given lower order modulation technique. It has been noticed that under fixed power allocation technique ADAPTIVE modulation scheme provides the lowest system BER in two-user model. While considering constrained optimization power allocation technique, both the system BER for ONLY BPSK and ADAPTIVE scheme almost provides same value. This is due to the power allocation coefficient which is optimally selected from a predefined allocation matrix to maintain a certain value of fairness factor. As the fairness level of achievable throughput of each user should be taken into consideration so that the throughput of those UEs approximately approaches to the same value, we

have selected different target fairness factor values, such as, 0.7 & 0.85, to compare the respective system BER plots. It is observed that for two-user model higher fairness factor value provides lowest BER under all the modulation schemes considered here, but while increasing the number of participating users in PD-NOMA from two to three higher fairness factor value provides higher system BER. This is because of the power allocation strategy to the users. The optimization algorithm which we have used here, consists of a predetermined power coefficient matrix which is very difficult to prepare. To improve this further the convex optimization technique can be applied where we can find out the required coefficients for each user.

The second part of the thesis deals with the real experimental study by implementing PD-NOMA in the WARP system successfully and then tested for performance analysis with respect to different modulation schemes to observe the difference between simulation and actual experimental studies in indoor fading environment. We have observed the PD-NOMA performance in terms of bit error rate with respect to transmit power considering various modulation techniques such as BPSK, QPSK and combination of BPSK-QPSK which is referred to as ADAPTIVE modulation scheme. One important difference between simulation and experimental study is the AGC which is the cardinal parameter in testbed to control BER. Further we have observed BER performance in two band : one in 2.4 GHz and the other in 5.0 GHz.

For two-user model with the target AGC gain -11 dBm in 2.4GHz range, system BER possesses the least value in case of ADAPTIVE modulation approach where the near user is provided with higher order modulation technique, i.e., QPSK and BPSK, a lower order modulation scheme, is imparted to the far user. It is also experimentally proved that power loss is more while considering 5GHz frequency band. Due to this reason system BER approaches the least value for ONLY-BPSK modulation scheme rather than ADAPTIVE approach under the consideration of

both the AGC target gain -8 dBm and -11 dBm. For three-user model the BER graphs exhibit better performance of system BER in case of ADPATIVE approach rather than ONLY-QPSK scheme. All the BER curves follow similar trend of water falling shape with respect to transmit power but shows a zigzag nature which reveals the fact of multipath propagation due to the indoor fading environment. The experimental test bed results exhibit the similar trend of BER curve validating the analysis of simulation in this thesis.

5.2 Future Scope:

- In chapter 4, the implementation of PD-NOMA is described up to three-user model. It can be extended up to only four-user model as each WARP kit provides only 4 RF ports for transmission as well as reception. It is one of the limitations of WARP board.

- The modulation schemes considered here are only BPSK and QPSK. Further research can be accomplished with different other higher order modulation techniques such as 8-PSK, 16-QAM, 64QAM and combination of those techniques to observe the effect on system BER.

- PD-NOMA technique can be implemented along with multiple input multiple output (MIMO) technology to explore the impact of diversity on the existing system.

- The BER graphs, which are the end results of our experiment, are not smooth water falling curve. Further research to explore novel channel estimation technique is needed to mitigate this effect.

References

[1]   J. G. Andrews, S. Buzzi, and W. Choi, *"What will 5G be?"* IEEE Journal on Selected Areas in Communications, vol. 32, no. 6, pp. 1065–1082, 2014

[2]   T. Rappaport, S. Sun, R. Mayzus et al., *"Millimeter wave mobile communications for 5G cellular: it will work!,"* IEEE Access, vol. 1, pp. 335–349, 2013.

[3]   E. G. Larsson, O. Edfors, F. Tufvesson, and T. L. Marzetta, *"Massive MIMO for next generation wireless systems,"* IEEE Communications Magazine, vol. 52, no. 2, pp. 186–195, 2014.

[4]   M. Kamel, W. Hamouda, and A. Youssef, *"Ultra-dense networks: a survey,"* IEEE Communications Surveys & Tutorials, vol. 18, no. 4, pp. 2522–2545, 2016.

[5]   S. Yang, P. Chen, L. Liang, Q. Bi and F. Yang, *"System design and performance evaluation for power domain non-orthogonal multiple access,"* 2015 IEEE/CIC International Conference on Communications in China (ICCC), 2015.

[6]   H. Sari, A. Maatouk, E. Caliskan, M. Assaad, M. Koca and G. Gui, *"On the foundation of NOMA and its application to 5G cellular networks,"* 2018 IEEE Wireless Communications and Networking Conference (WCNC), 2018, pp. 1-6.

[7]   Z. Ding, P. Fan, and H. V. Poor, *"Impact of User Pairing on 5G Nonorthogonal Multiple-Access Downlink Transmissions,"* IEEE Transactions on Vehicular Technology, vol. 65, no. 8, pp. 6010–6023, 2016.

[8]   S. Timotheou and I. Krikidis, *"Fairness for Non-Orthogonal Multiple Access in 5G Systems,"* IEEE Signal Processing Letters, vol. 22, no. 10, pp. 1647–1651, 2015.

[9]   Z. Yuan, G. Yu, and W. Li, "Multi-User Shared Access for 5G," Telecommunications Network Technology, vol. 5, no. 5, pp. 28– 30, May 2015.

[10]   H. Nikopour and H. Baligh, *"Sparse code multiple access,"* in Proceedings of the IEEE 24th Annual International Symposium on Personal, Indoor, and Mobile Radio Communications (PIMRC '13), pp. 332–336, IEEE, London, UK, September 2013.

[11]   R. Hoshyar, F. P. Wathan, and R. Tafazolli, *"Novel low-density signature for synchronous CDMA systems over AWGN channel,"* IEEE Transactions on Signal Processing, vol. 56, no. 4, pp. 1616–1626, 2008.

[12]   J. Zeng, D. Kong, X. Su, L. Rong, and X. Xu, *"On the performance of pattern division multiple access in 5G systems,"* in Proceedings of the 8th International Conference on Wireless Communications and Signal Processing, WCSP 2016, pp. 1–5, Yangzhou, China, October 2016.

[13]   J. Huang, K. Peng, C. Pan, F. Yang, and H. Jin, *"Scalable video broadcasting using bit division multiplexing,"* IEEE Transactions on Broadcasting, vol. 60, no. 4, pp. 701–706, 2014.

[14]   L. Dai, B. Wang, Y. Yuan, S. Han, C. I, and Z. Wang, *"Nonorthogonal multiple access for 5G: solutions, challenges, opportunities, and future research trends,"* IEEE Communications Magazine, vol. 53, no. 9, pp. 74–81, 2015.

[15]   *"Study on downlink multiuser superstition transmission (MUST) for LTE (Release 13),"* Tech. Rep. 3GPP TR 36.859, 2015.

[16]   *"Evaluation methodologies for downlink multiuser superposition transmissions,"* Tech. Rep. 3GPP R1-153332, NTT DOCOMO Inc., Fukuoka, Japan, May 2015.

[17]   *"Deployment scenarios for downlink multiuser superposition transmissions,"* Tech. Rep. 3GPP R1-152062, NTT DOCOMO Inc., Belgrade, Serbia, April 2015.

[18]   *"Candidate non-orthogonal multiplexing access scheme,"* Tech. Rep. 3GPP R1-153335, MediaTek Inc., Fukuoka, Japan, May 2015.

[19]   *"System-level evaluation results for downlink multiuser superposition schemes,"* Tech. Rep. 3GPP R1-154536, NTT DOCOMO Inc., Beijing, China, August 2015.

[20]   *"Link-level evaluation results for downlink multiuser superposition schemes,"* Tech. Rep. 3GPP R1-154537, NTT DOCOMO Inc., Beijing, China, August 2015.

[21]   *"New work item proposal: Downlink multiuser superposition transmission for LTE,"* Tech. Rep. 3GPP R1-160680, MediaTek Inc., Gothenburg, Sweden, March 2016.

[22]   L. Zhang, W. Li, Y. Wu et al., *"Layered-Division-Multiplexing: Teory and Practice,"* IEEE Transactions on Broadcasting, vol. 62, no. 1, pp. 216–232, 2016.

[23]   *"New study item proposal: study on non-orthogonal multiple access for NR,"* Tech. Rep. 3GPP RP-170829, ZTE-CATT-IntelSamsung, Dubrovnik, Croatia, March 2016.

[24]   S. Vanka, S. Srinivasa, Z. Gong, P. Vizi, K. Stamatiou, and M. Haenggi, *"Superposition coding strategies: Design and experimental evaluation,"* IEEE Trans. Wireless Commun., vol. 11, no. 7, pp. 2628–2639, 2012.

[25]   Mahmoud Aldababsa, Mesut Toka, Selahattin Gökçeli, Güneş Karabulut Kurt, Oğuz Kucur, *"A Tutorial on Non Orthogonal Multiple Access for 5G and Beyond"*, Wireless Communications and Mobile Computing, vol. 2018, Article ID 9713450, 24 pages, 2018.

[26]   Theodore S. Rappaport. *Wireless Communications Principles and Practice* (2nd ed.). Pearson, 2010.

[27]   Amiri, Karim & Sun, Yang & Murphy, Patrick & Hunter, Christopher & Cavallaro, Joseph & Sabharwal, Ashutosh. (2007*). WARP, a Modular Testbed for Configurable Wireless Network Research at Rice.*

[28]   http://www.gnu.org/software/gnuradio

[29]   http://www.sundance.com

[30]   http://www.lyrtech.com

[31]   Rami Akeela, Behnam Dezfouli, *"Software-defined Radios: Architecture, state-of-the-art, and challenges"*, Computer Communications 128 (2018) 106–125, Elsevier

[32]   Vigneswara Rao Gannapathy, Ahamed Fayeez Bin Tuani Ibrahim, Zahriladha Bin Zakaria, Abdul Rani Bin Othman , Nur Qalbi Binti Jalaudin, *"A Review on Various Types of Software Defined Radios (SDRS) in Radio Communication",* International Journal of Research in Engineering and Technology, · December 2014

[33]   Z. Tong, M. S. Arifianto, and C. F. Liau, *"Wireless Transmission using Universal Software Radio Peripheral,"* Int. Conf. Sp. Sci. Commun. 2009, pp. 19– 23, 2009.

[34]   N. B. Truong and C. Yu*, "Investigating Latency in GNU Software Radio with USRP Embedded Series SDR Platform,"* 2013 Eighth Int. Conf. Broadband Wireless Comput. Commun. Appl., pp. 9–14, Oct. 2013.

[35]   https://mangocomm.com/products/kits/warp-v3-kit/

[36]   http://warpproject.org/trac/wiki/GettingStarted/WARPv3/Hardware

[37]   https://warpproject.org/trac/wiki/GettingStarted/WARPv3/IntroToTools

[38]   https://warpproject.org/trac/wiki/WARPLab

[39]   https://warpproject.org/trac/wiki/Exercises/FPGABoardIntro/UsingImpact

[40]   https://warpproject.org/trac/wiki/howto/SPI_Flash_Config

[41]   Titiek Suryani, Suwadi, Hasan, Septriandi Wira Yoga, *"Implementation and Performance Evaluation of Orthogonal Frequency Division Multiplexing (OFDM) using WARP"*, 2015 International Seminar on Intelligent Technology and Its Applications.

[42]   Mahsa Shafiee, Kyle O'Keefe, Gérard Lachapelle, *"Symbol Timing Acquisition for Collaborative OFDM WLAN-based A-GPS"*, Springer International Journal of Wireless Information Networks, June 2013

[43] Schmidl, Timothy M., and Donald C. Cox. *"Robust frequency and timing synchronization for OFDM."* Communications, IEEE Transactions on 45.12 (1997)

[44] Speth, Michael, et al. *"Optimum receiver design for wireless broad-band systems using OFDM. I."* Communications, IEEE Transactions on 47.11 (1999).

[45] https://warpproject.org/trac/wiki/WARPLab6/Specifications

[46] https://warpproject.org/trac/wiki/WARPLab/AGC

[47] https://warpproject.org/trac/wiki/WARPLab/Reference/Interface/X245